Impact of Multimeric Ferrocene-containing Cyclodecapeptide Scaffold on Host-Guest Interactions at a β-Cyclodextrin Covered Surface

Enrique Sanchez Perez, Ritu Toor, Pierrick Bruyat, Céline Cepeda, Mélissa Degardin, Jérôme Dejeu, Didier Boturyn, Liliane Coche-guérente

Impact of multimeric ferrocene-containing cyclodecapeptide scaffold on host-guest interactions at a β-cyclodextrin covered surface

Enrique Sanchez Perez, Ritu Toor, Pierrick Bruyat, Céline Cepeda, Mélissa Degardin, Jérôme Dejeu, Didier Boturyn*, Liliane Coche-Guérente*

Dr. E. Sanchez Perez, Dr. R. Ritu, Dr. P. Bruyat, Dr. C. Cepeda, Dr. M. Degardin, Dr. J. Dejeu, Dr. Boturyn, Dr. L. Coche-Guérente,
Department of Molecular Chemistry
Univ. Grenoble-Alpes, CNRS, DCM UMR 5250,
CS 40700, 38058 Grenoble Cedex 9, France
E-mail: liliane.guerente@univ-grenoble-alpes.fr; didier.boturyn@univ-grenoble–alpes.fr

Supporting information for this article is given via a link at the end of the document.

Abstract: Among non-covalent bonds, the host-guest interaction is an attractive way to attach biomolecules to solid surfaces since the binding strength can be tuned by the nature of host and guest partners or through the valency of the interaction. For that purpose, we synthesized cyclodecapeptide scaffolds exhibiting in a spatially controlled manner two independent domains enabling the multimeric presentation of guest molecules on one face and the other face enabling the potential grafting of a biomolecule of interest. In this work, we were interested in the β-cyclodextrin/ferrocene inclusion complex formed on β-CD monolayers functionalized surfaces. By using surface sensitive techniques such as quartz crystal microbalance and surface plasmon resonance, we quantified the influence of the guest valency on the stability of the inclusion complexes. The results show a drastic enhancement of the affinity with the gradual increase of guest valency. Considering that the sequential binding events are equal and independent, we applied the multivalent model developed by the group of Huskens to extract intrinsic binding constants and an effective concentration of host.

Introduction

Non-covalent interactions between host and guest molecules are often exploited for a wide range of biological applications such as injectable hydrogels, drug delivery materials and functionalization of surfaces for the study of cell adhesion.[1,2] These interactions are based on the temporary association of a host molecule exhibiting a cavity (e.g. calixarenes, cyclodextrins, cucurbit[n]urils) with a suitable molecular guest. Host-guest interactions are particularly suitable for surface functionalization *via* immobilization of functional molecules. In the context of cell adhesion platform, the arginine-glycine-aspartic acid (RGD) peptide sequence, which is found in the extracellular matrix proteins, has been extensively exploited to design artificial adhesive surfaces.[3] It has been shown that the choice of RGD-containing guest molecules modulates the cell behavior.[4] It is now recognized that the host-guest supramolecular chemistry is a method of choice for the design of dynamic synthetic biointerfaces opening new opportunities in the field of biomedical sciences.[5] Reversible host-guest interactions are especially well-adapted for the dynamic control over bioactivity on surfaces allowing the possible sensor reuse. The first example of a host-guest system applied to the electrochemical control of living cells attachment/detachment process was designed by Q. An *et al.* [6] The host compound cucurbit[8]uril is able to bind two aromatic guest molecules, one of them displaying a linear RGDS peptide. L. Yang *et al.* reported the immobilization of a divalent ferrocene-tagged protein onto β-CD-modified surface and demonstrated the reversibility of the adsorption upon oxidation of the ferrocene moieties.[7] By taking into account the advantages of such reversibility, P.H. Schwartz *et al.* immobilized adamantylated proteins to a β-CD monolayer functionalized gold surface.[8] The addition of an excess of competitive adamantine guest molecule in solution triggered the release of bound proteins. In our group, we are particularly interested in the β-cyclodextrin/ferrocene (β-CD/Fc) inclusion complex as it is able to dissociate under mild electrochemical polarization. Previously, we designed functionalized surfaces that permit a selective tumor cell capture and release.[9,10] As the β-CD has a weak binding affinity for ferrocene (K_A close to 10^3 M^{-1}),[11] we have exploited a nano-sized cyclopeptide scaffold composed of ten amino acid residues that present in a spatially controlled manner two independent functional domains:[12] a ligand domain for cancer cell recognition and a clustered Fc domain allowing host-guest interactions through a multivalent presentation.[9,10] Multivalent interactions are known to be much stronger than the corresponding monovalent ones,[13] in particular at interfaces.[14] This was highlighted by the group of Huskens that studied the multivalency effect of Fc-containing dendrimers on β-CD-modified self-assembled monolayers (SAMs) surfaces.[15] Although increasing the number of interaction enhances the binding, the scaffold architecture can strengthen or weaken the interaction.[16] Among multivalent structures, dendrimers and small templates (calixarene, cyclopeptide) offer unique properties such as their nanometer size and the control of ligand number that make them particularly attractive for a wide range of applications.[17]

In this context, further studies are required to gain a better understanding of the effect of multivalency based-cyclodecapeptide scaffold on the host-guest interaction strength.

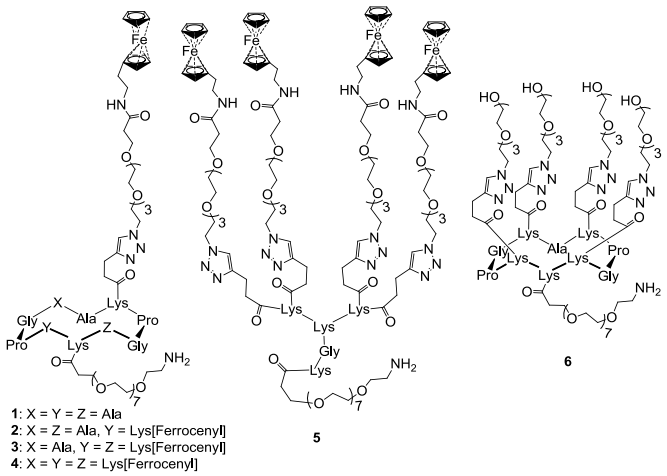

Figure 1. Design of compounds **1** to **6**.

We then synthesized cyclodecapeptides bearing between one to four Fc units and a Fc-containing polylysine dendrimer in order to illustrate the influence of the pre-organized architecture of the cyclopeptide template (Figure 1). The characterization of the interactions between Fc-containing peptides and β-CD monolayer is achieved by using label-free surface sensitive techniques such as quartz crystal microbalance with dissipation monitoring (QCM-D) and surface plasmon resonance (SPR). QCM-D and SPR are able to probe the binding and interactions of analyte with a functionalized sensor chip under dynamic conditions and in real time. QCM-D provides the hydrated mass of the deposit whereas SPR provides the kinetic and thermodynamic parameters of the interaction between β-CD monolayer and Fc-containing compounds. Our results show that a gradual increase of Fc valency induces a drastic enhancement of the affinity for Fc-containing scaffold whereas the polylysine dendrimer exhibits high non-specific interaction with β-CD-SAM.

Results and Discussion

Design of β-cyclodextrin (β-CD) functionalized surfaces. We previously reported the host properties of β-CD SAMs on gold surface formed by the selective grafting of a monofunctionalized β-CD derivative on a preformed SAM *via* copper(I)-catalyzed alkyne-azide cycloaddition reaction, allowing a perfect control of the amount and accessibility of the immobilized β-CD cavities.[10,18-20] In the present work, the construction of β-CD SAM has been simplified in order to shorten the preparation time. It consists in a "one step" procedure exposing directly the gold surface to a mixed solution of β-CD-terminated thiol (CD-thiol) and oligo(ethylene glycol)-terminated thiol (hydroxyl-thiol) used as a diluent.[9,20] Wettability studies were carried out by measuring contact angles of water on SAM surfaces previously exposed to various molar ratios of CD-thiol in order to analyze the variation of the surface hydrophilicity. The stepwise increase from 0 to 5% of the CD-thiol molar ratio in the thiol solution from which the β-CD SAMs were formed is accompanied by a continual decrease of the contact angles (from 36±4 deg. to 25±4 deg.) whereas for molar ratios higher than 10%, constant values of the contact angles were measured 22.5±1.5deg. (Figure S1, ESI). This observation suggests that the number of surface-attached β-CD is correlated to the CD-thiol molar ratio in the thiol mixture used to prepare the SAMs. In the case of the previously reported "two steps" procedure, the β-CD surface density was controlled by the molar ratio of the azide-thiol in the thiol mixture from which the SAMs were formed. The stable wettability of the modified surface above 10% of CD-thiol could be indicative of a saturation of the β-CD surface assuming a close-packed monolayer of β-CD tori.

In order to characterize the structure of β-CD SAM constructed from the "one-step" procedure, we used electrochemical techniques as they are highly sensitive to nanometer scale monolayers defects. In particular, we aimed to confirm the absence of defects which would suggest a low packing density and an unfavorable orientation of the β-CD torus. Indeed, it has been reported that the formation of a densely packed β-CD monolayer on gold surface required more than one attachment point (until seven sulfur-bound have been used) or fill the space left under the β-CD tori with short alkane thiols.[21-24] Electrochemical capacitance provides information on the macroscopic permeability of the SAM assemblies. By recording cyclic voltammograms in 0.2 M Na_2SO_4 for different scan rates from 0.05 to 5 V/s, we measured the capacitive current and extracted the double layer capacitance for gold functionalized with 100% of hydroxyl-thiol, 20% of CD-thiol and bare gold (Figure S2A, ESI). We found a capacitance of 9.6±0.5 µF/cm^2 for β-CD SAM closed to that of hydroxyl-SAM (6.4±0.3 µF/cm^2) while a value of 20.9±0.8 µF/cm^2 was measured on bare gold. The double layer capacitance of β-CD SAM is in accordance with those reported in the literature.[21,23] In addition, we evaluated the permeability of β-CD SAM towards a diffusing redox probe $Fe(CN)_6^{3-}$ in comparison with hydroxyl-SAM (Figure S2B, ESI). The absence of faradaic current on the two SAM-functionalized surfaces is indicative of the integrity of the assemblies. The two latter results, i.e. low double layer capacitance and gold surface passivation, evidenced of an absence of defects sites or pinholes of the β-CD SAM. Such behavior originated from the composition of the mixed SAM which results from the assembly of two long alkyl chain.

Characterization of host-guest properties using QCM-D. To study the host properties of β-CD SAM surface, we analyzed the capabilities of the β-CD-modified surface to capture Fc guest molecules. The Fc-containing cyclodecapetide scaffolds **1** to **4** bearing 1 to 4 Fc respectively and polylysine dendrimer **5** bearing 4 Fc (Figure 1) were prepared according to previously reported procedures by a combination of a standard solid-phase and solution peptide synthesis procedures (see ESI for more details and characterization).[10,25] QCM-D has been selected to evaluate the hydrated mass of ferrocene guest molecules trapped in the cavities of the β-CD SAMs on the sensor surface. The experiments were first achieved by using a cyclodecapeptide scaffold bearing four ferrocene groups (compound **4**) and β-CD saturated-surface.

Figure 2A shows the immobilization of Fc-containing compound **4** on β-CD SAM prepared from thiols mixture (20 mol% of thiol-CD). As expected, the Fc-containing compound **4** did not interact with a SAM surface without β-CD (Figure S3A, ESI).

Additionally, a cyclodecapeptide control compound **6** without guest molecules did not adsorb on the β-CD SAM (Figure S3B, ESI). These experiments proved the binding selectivity of the guest molecules captured by the β-CD cavities forming inclusion complexes.

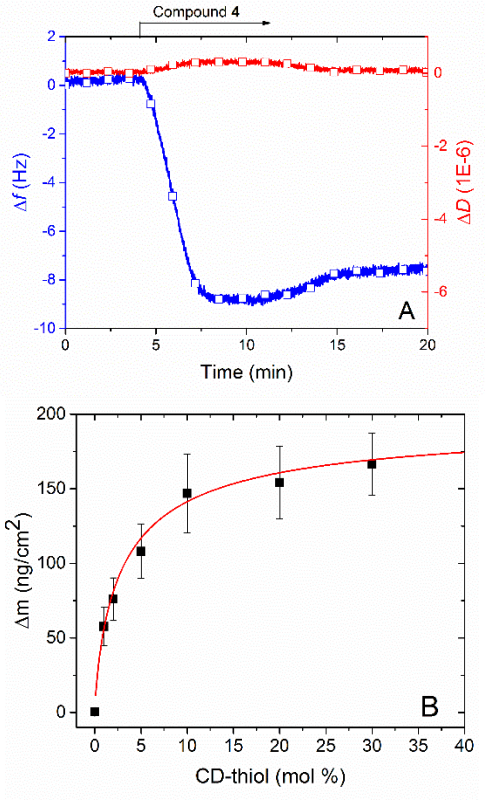

Figure 2. (A) QCM-D signals (frequency shifts in blue, dissipation shifts in red) recorded during the adsorption of 5 µM Fc-containing compound **4**. Start and duration of incubation step with the compound **4** is indicated by arrow; during all other time, the surface was exposed to buffer solution (T = 24°C, flow rate = 10 µL.min^{-1}). (B) Hydrated mass (calculated by using Sauerbrey equation considering a rigid layer) of compound **4** adsorbed on β-CD SAM surface as a function of CD-thiol molar ratios in the solution from which the SAMs were formed (the error bars have been calculated from a minimum of four QCM-D experiments).

The low softness of the layer (corresponding to a low dissipation shift) as shown by the QCM-D profile (Figure 2A), enables the calculation of the hydrated mass by using the Sauerbrey equation (5). We thus obtained a mass uptake of 162 ± 28 ng/cm^2 and 147 ± 26 ng/cm^2, respectively before and after rinsing. We noticed a weak release of guest compound upon rinsing step followed by stable signals. The hydrated masses could be compared to the molecular surface density which had been previously measured [9] by spectroscopic ellipsometry for similar Fc-containing scaffolds, we reported values of 22 pmol/cm^2 (83.4 ± 7.0 ng/cm^2 before rinsing) and 18.6 pmol/cm^2 (70.3 ± 5.9 ng/cm^2 after rinsing). By comparing the dry masses with the hydrated ones extracted from QCM-D measurements, hydration ratios of 49% and 52% were respectively obtained.

Following the characterization of the host properties of β-CD saturated-surface, we carried out QCM-D experiments monitoring the formation of inclusion complex on β-CD SAM surface as a function of host (β-CD) surface densities. The graph in figure 2B shows similar trend as that observed from contact angle measurements, *i.e.* a first increase and then stabilization for values higher than 10%. These results show that the amount of guest molecule adsorbed on the host layer could be controlled by the CD-thiol molar ratio in the solution from which the mixed SAMs were formed. It is important to note that the SAMs prepared *via* a "one-step" procedure exhibit similar host properties than the SAMs prepared *via* a "two-steps" procedure reported previously, involving the covalent coupling of β-CD on a preformed azide-SAM (Figure S4, ESI).[9] We can conclude that the packing densities of the host monolayers resulting from "one step" or "two steps" procedures are similar. Regarding the compound **4** surface coverage on a β-CD saturated-surface which has been measured by spectroscopic ellipsometry (19 pmol/cm^2) and reported previously, it corresponds to about one fourth of the

estimated surface concentration by considering hexagonally close-packed β-CDs with a flat orientation (75 pmol/cm^2).[21] This result was confirmed by cyclic voltammetry experiment using the redox properties of Fc (Fig. S5, ESI). The determination of the anodic charge associated with the conversion of Fc to its oxidized state Fc$^{\cdot+}$ enables the calculation of a Fc surface coverage of 73 pmol/cm^2 (for calculation, see ESI). Comparable host coverage were measured for β-CD monolayers prepared from the "two step" procedure by titration performed at varying concentrations of guest.[18] The size of a cyclopeptide scaffold has been reported to have a rectangle-like shape of 11.2 ± 0.6 Å and 4.95 ± 0.25 Å[26] bearing pendant ferrocene moieties with an average distance between them of 21.3 Å.[27] It results the calculation of a footprint of about 4.5 nm^2 for the tetravalent guest molecule. By comparison with the estimated size of the β-CD torus (leading to a surface area of 1.8 nm^2)[21] we could assume of a possible formation of three or four Fc-β-CD interactions.
In order to analyze the influence of the Fc number on the stability of the inclusion complexes, we studied the adsorption of Fc-containing guest molecules on monolayers fully covered with β-CD (resulting from the incubation of gold surface in thiols mixture containing 20 mol% of CD-thiol). Table 1 shows the comparison of the shifts in resonance frequency for all the Fc-containing scaffolds (for compounds **4** to **1**, bearing 4 to 1 Fc moieties respectively and dendrimer **5** bearing 4 Fc) before and after rinsing the functionalized quartz crystal.

Table 1. QCM-D data for the adsorption of Fc-containing compounds.

Compounds[a] (Mw g/mol)	$-\Delta f_1$ (Hz) (before rinsing)	$-\Delta f_2$ (Hz) (after rinsing)
4 (3779)	9.0 ± 1.5	8.2 ± 1.4
5 (3340)	11 ± 2[b]	8.6 ± 1.7
3 (3134)	8.5 ± 1.4	6.3 ± 1.8
2 (2497)	8 ± 1.3	2 ± 0.8
1 (1855)	2 ± 1[c]	1 ± 0.7

[a] The Fc-containing scaffolds have been injected with a concentration of 5µM excepted for compound **1**, a concentration of 50 µM has been used.

[b] Dendrimer **5** bearing 4 Fc, the signal drift makes the measurement inaccurate, the shift in frequency has been measured after about 20 min of adsorption [c] As a continuous signal drift is observed, the shift in frequency has been measured after about 20 min of adsorption.

Whereas compound **3** displays the same behavior as compound **4** (Figure S6, ESI), we noticed a marked difference for compound **2** as shown the QCM-D profile in Figure 3. After rinsing of the measurement chamber, QCM-D profile exhibits a slow but significant positive shift in frequency until about - 2 Hz, characterizing an important release of the bivalent guest attributed to a low apparent affinity of **2** for β-CD SAM monolayer. For compound **1** an injection of 5 µM did not show any shift in frequency, the observation of significant adsorption requires a concentration ten times higher. But even at 50 µM, the change in frequency did not reach a plateau, the signal is decreasing continuously but remains very low (Figure S7, ESI). Regarding the adsorption of dendrimer **5**, the shift in frequency is similar to that obtained for the cyclodecapeptide **4** (Table 1) (Figure S8, ESI). The difference relies on the absence of a plateau shape following the initial fast shift in frequency. A weak negative drift of the frequency has then been noticed with a slope of -0.16 Hz/min. Such behavior should be indicative of non-specific adsorption on β-CD monolayer.

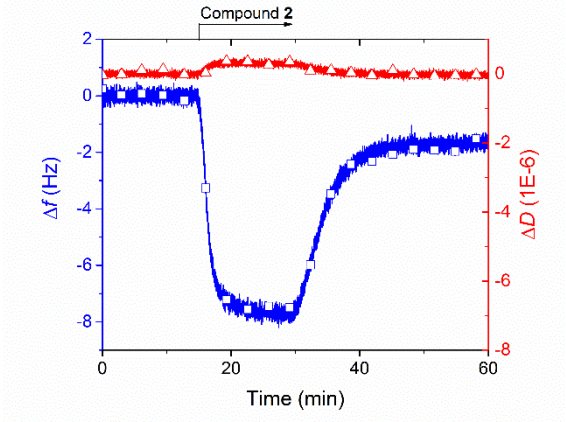

Figure 3. QCM-D profile (frequency – blue, dissipation – red) recorded during the adsorption of 5 µM Fc-containing compound **2**. Start and duration of incubation step with the compound **2** is indicated by arrow; during all other time, the surface was exposed to buffer solution

These results highlight the benefit of multimeric systems: while compounds bearing 3 and 4 Fc residues form stable inclusion complexes, a dramatic fall in apparent affinity was observed for compound **2**, the monomeric Fc-compound **1** having very weak adsorption.

Characterization of the Fc-containing compounds affinity by using SPR. To further study the affinity of the Fc-containing compounds, we performed kinetic binding analysis by SPR. The sensorgrams of compounds **2** and **4** recorded on the same β-CD-saturated SAM surface show similar trends as in QCM-D: a much lower dissociation phase is observed for compound **4** compared to compound **2** (Figure S9, ESI). Altogether QCM-D and SPR analyses provide qualitative information in the binding affinity of the compounds **1**-**5**. In terms of reversibility of the adsorption, the two techniques bring the same result, compound **2** is reversibly adsorbed on the β-CD surface compared to compound **4**. SPR provides quantitative informations allowing to extract the thermodynamic and kinetic parameters of the host-guest interactions. We checked the absence of non-specific adsorption of the supramolecular compounds on hydoxyl-SAM surface. Such evaluation is essential because the SPR sensor chip is uniformly covered with β-CD SAM leading to the formation of four identical flow cells without the possibility of drawing a reference cell. All sensorgrams exhibit a small refractive index effect which is restored by rinsing the microfluidic cell with the buffer solution (Figure S10, ESI). The incubation of Fc-containing supramolecular compounds **1**-**4** on hydroxyl-SAM (without β-CD) showed an absence of non-specific adsorption while the dendrimer **5** presented an abnormal behavior. During the contact time of the sensor chip with Fc-containing dendrimer the SPR signal did not exhibit a plateau but a continuous positive drift. After the rinsing step the magnitude of the signal did not recover the initial baseline. Such behavior can be attributed to a non-specific adsorption of dendrimer **5**.

The SPR analysis of the Fc-CD interaction required a method of surface regeneration enabling the complete dissociation of the inclusion complex and the regeneration of β-CD SAM. To this end, a chemical oxidation of Fc guest was carried out by an oxidized solution of ferrocenylmethanol Fc^+-OH (Figures S11 and S29, ESI). The regeneration procedure appeared inefficient for dendrimer **5** (Figure S11, ESI). Indeed around 30% of **5** remained adsorbed to the surface. This abnormal behavior is attributed to the non-specific interaction between dendrimer **5** and the SAM monolayer which makes the chemical oxidation inefficient (Figure S11, ESI). Such high non-specific adsorption could be due to the entrapment of flexible polylysine Fc-terminated arms inside the SAM layer.

The binding affinities of Fc-containing supramolecular compounds were then determined by fitting the SPR data recorded at various concentrations using a 1:1 Langmuir model (Figure 4B). In the case of very high affinity and for very low concentrations, the steady-state equilibrium was not reached during the contact time allowed by the Biacore program (maximum 420 s for a flow rate of 50 µL/min). Such behavior is depicted by sensorgrams of figure 4A: for concentrations lower than 50 nM for compound **4**, the plateau was not reached. To circumvent this hurdle, we carried out multiple successive injections of the same concentration until reaching a plateau working under manual run and we collected the SPR binding assays exclusively for concentrations leading to steady-state equilibrium. An example of such procedure is shown in the supporting information (Figure S12, ESI).

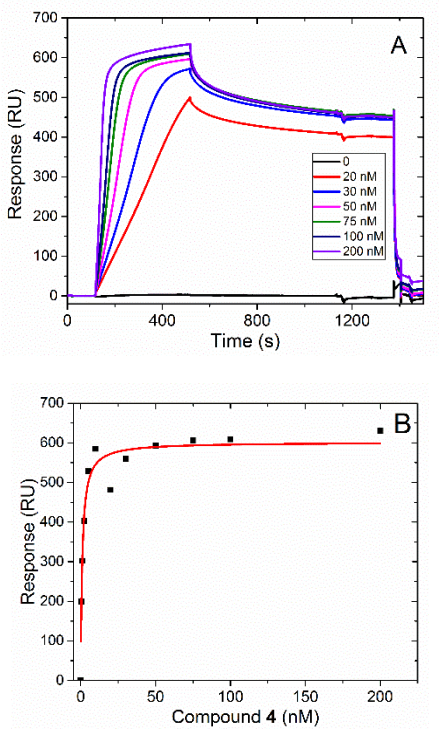

Figure 4. (A) Kinetic binding assays for compound **4** of concentrations range from 20 to 200 nM; (B) Langmuir isotherm leading to extract a K_D value of 1 nM.

The Langmuir isotherms relative to compounds **2** and **3** are presented in the supporting information (Figure S13, ESI). Due to the high level of non-specific interaction of dendrimer **5**, its binding constant was not determined. All the other apparent K_D of Fc-containing scaffolds determined by using Langmuir isotherm (K_D thermo) are depicted in table 2. Data show an increase of the apparent binding affinity with the Fc valency. Regarding the monovalent compound **1**, as it was not possible to work with solutions of concentrations

higher to 50 µM due to a lack in solubility, we could only estimate a K_D value using the steady-state equilibrium on experimental sensorgrams (Figure S14, ESI).

Table 2. Parameters characterizing the interaction of Fc-containing supramolecular compounds with β-CD surface

Compound	n (guest number)	K_D (Thermo)	β[a] (avidity factor)	α[b] (degree of cooperativity)
1	1	130 ± 30 (µM)	1	1
2	2	2 ± 1 (µM)	65	0.74
3	3	15 ± 5 (nM)	$8.7\ 10^3$	0.67
4	4	1.0 ± 0.5 (nM)	$1.3\ 10^5$	0.58

[a] $\beta = K_A^{poly,n}/K_A^{mono}$ with $K_A^{mono} = 1/K_D$; [b] $\alpha = Ln(K_A^{poly,n})/Ln(K^{mono})^n$

We found an apparent K_D of about 130 µM for the monovalent interaction in accordance with published results demonstrating that the equilibrium constant for inclusion complex between Fc and β-CD at surface is one order magnitude greater than that in solution.[28] Such difference has been explained by the decrease of the entropy factor due to the immobilization of β-CD.[28] The enhancement of the affinity accompanying the increase of the ligand number can be characterized by the avidity factor α defined by Whitesides *et al.* [29] Table 2 shows that the values of β is equal to 65 for a valency of 2 using the equation (1) below and reach 10^5 for a valency of 4:

$$\beta = \frac{K_A^{poly,n}}{K_A^{mono}} \qquad (1)$$

$K_A^{poly,n}$ is the global equilibrium association constant and K_A^{mono} is the monomeric equilibrium association constant. The gain in affinity could also be discussed in terms of free energies. Whitesides *et al.* defined a degree of cooperativity, the factor α (2): [29]

$$\propto = \frac{\Delta G^{poly}}{n \times \Delta G^{mono}} \qquad (2)$$

n is the number of Fc guest per scaffold (see ESI). Table 2 shows that α is decreasing drastically for valencies of 3 and 4. A degree of cooperativity lower than 1 (from 0.74 for n=2 to 0.58 for n=4) can be interpreted by a slight negative cooperativity as the binding of the first ligand could impede the binding of the second ligand. The group of Huskens quantitatively addressed the thermodynamic and kinetic issues related to the use of multiple interactions of guest-containing molecules at β-CD SAMs surfaces.[30,31] They developed a general model aiming to study the multivalent interactions at surfaces. In this model, the sequential binding events are considered equal and independent. Consequently all binding constants can be expressed in terms of intrinsic binding constants $K_{i,s}$ and effective concentration C_{eff} of CD host. The maximum effective concentration ($C_{eff,max}$) represents the number of accessible host sites in the probing volume of a non-attached guest site upon binding of a first guest site belonging to a multivalent scaffold. The cooperativity on the surface is only viewed as an increase of the effective concentration upon binding of the first guest site. The interaction strength of an individual host-guest interaction on the surface characterized by $K_{i,s}$ has been shown to be close to that in solution $K_{i,l}$. The relation between multivalent and monovalent binding is given by the equation (3) below:[31]

$$K_A = C_{eff,max}^{(n-1)}\ K_{i,s}^n \qquad (3)$$

K_A is the overall binding constant, $C_{eff,max}$ is the maximum effective concentration and n is the valency of the host-guest interaction. $C_{eff,max}$ has been assumed to be independent of the number of guest binding sites and only dependent of the guest molecular geometry and the number of hosts on the surface. Thus $C_{eff,max}$ can be estimated from the linker length between two guest sites within the multivalent scaffold using the following equation (4):[31]

$$C_{eff,max} = \frac{\pi\ L^2\ N_{Av}\ \Gamma_s - 1}{\left(\frac{2}{3}\right)\pi\ N_{Av}\ L^3} \qquad (4)$$

L is the linker length between two guest sites on the scaffold. Based on previous work concerning the conformational studies of a similar scaffold bearing four recognition elements (cyclopentapeptide) and the same linkers, we could estimate the distance between two guest sites. An inter-recognition element distance between 1.38 and 2.85 nm was determined by molecular dynamics.[27] By transferring these values to the calculation of $C_{eff,max}$, we obtained effective concentrations between 0.57 and 0.39 M, respectively. From the overall binding constants obtained by using a Langmuir model (assuming 1:1 binding) and the estimated $C_{eff,max}$, intrinsic binding constants $K_{i,s}$ could be extracted for each compound (Table S1, ESI). As $K_{i,s}$ were found lower for **3** and **4** (as about one magnitude order) than $K_{i,l}$ ($10^3\ M^{-1}$) we could conclude to a negative slight cooperativity. In addition, we noticed a small decrease of $K_{i,s}$ with the increase of the valency, from 1090 M^{-1} for compound **2** to 272 M^{-1} for compound **4**. In order to exclude the use of the estimated value of $C_{eff,max}$ for the determination of $K_{i,s}$, we applied the multivalent model developed by Huskens *et al*. to fit the experimental SPR data.[31] To this end, the theoretical model was adapted to our experimental conditions including: (i) absence of monovalent competitor (β-CD) in solution, (ii) a concentration of free guest in solution equal to the total guest concentration injected as we made the assumption that in the Biacore

microfluidic set-up the concentration of host-guest complexes is negligible compared to the concentration of flowing guest (Figure S15, ESI).[31]

Table 3. Binding parameters extracted from the fitting data of the SPR responses as a function of the injected concentrations of Fc-containing scaffolds[a] (Figure S14).

Com-pound	$K_{i,s}$ (M^{-1})	C_{eff} (M)	R_{max} (RU)	R_{max}/M_w	$1/P_{av}$[b]	R[c]
2	823	0.34	997	0.4	1.99	0.999
3	566	0.33	496	0.16	2.97	0.996
4	281	0.34	598	0.16	3.98	0.996

[a]: compound 1 was not evaluated because of its low solubility and affinity.

[b]: p_{av} represents the average number of interactions used by a guest molecule to bind to the surface.

[c]: R is the correlation factor of the fitting data.

Table 3 presents the fitting of the SPR data and shows $K_{i,s}$ values of the same magnitude order as those determined by using estimated values of $C_{eff,max.}$ The latter result confirms the slight negative cooperativity of the interaction. It should be noted that this slight negative cooperativity does not hamper the multivalent effect. The fitted parameter, C_{eff} was found to be close to 0.34 M, a value slightly lower to the previous calculated value of $C_{eff,max}$. Considering that C_{eff} must be close to $C_{eff,max}$, we expected a much higher difference between the fitted value of C_{eff} and $C_{eff,max}$ calculated from an estimated inter-ligand distance. A $C_{eff,max}$ of 0.34 M should correspond to distance of 3.3 nm. From the fitted parameter $1/p_{av}$ which depends on the binding stoichiometry of the interaction, we assume that each Fc of the multivalent scaffold binds to the β-CD receptor confirming the result observed from electrochemical study using compound **4**. Regarding R_{max} values and especially the ratio R_{max}/Mw which depends on the surface coverage of Fc-containing scaffold bound to saturated β-CD surface, the same ratio for compounds **3** and **4** was determined (Table 3). This result demonstrates that the same number of scaffolds was adsorbed on the β-CD surface. In the case of compound **3,** due to the steric hindrance of the scaffold, not all β-CD receptors were bound to a Fc guest probably. As a result, we expect for tri- and tetravalent molecules an adsorption in a parallel plane, whereas in the case of the bivalent one (with two ferrocene on the same side) the bound scaffold could be immobilized in a perpendicular plane towards the gold surface. In this architecture the ratio (R_{max}/Mw) for **2** should be between 0.32 and 0.43 (considering that three Fc guests block one CD host per multivalent compound), which is in accordance with the experimental data (0.4, Table 3).
The surface coverage of the β-CD-SAM is comparable to the "molecular printboard" described by the group of Huskens, which expose the hydrophobic cavities of β-CD in a hexagonal lattice to the buffer solution. Consequently, the difference in the binding strength could be ascribed only to the geometry and rigidity of the guest-containing scaffold. The lack of flexibility of the cyclodecapeptide scaffold can impede the binding of the second, third or fourth guest sites after the binding of the first one. Advantageously, unlike the flexible polylysine dendrimer, the rigidity of the cyclodecaptide scaffold limits significantly non-specific interactions with a great potential for biological applications. We previously demonstrated the benefit of such structure for cell capture on different surfaces by grafting tumor cell ligand (RGD peptide) and anchoring surface systems (Biotin, Fc) on each side of the scaffold.[9,10,32]
In order to go further in the characterization of the present host-guest interactions, we determined the kinetic parameters, *i.e.* the association (k_{on}) and dissociation (k_{off}) rate constants. Due to the weak dissociation of the complex formed for high valency, only the association phase of the curves can be fitted. In this context, the fitting of experimental data cannot be performed using the classical kinetic models from Biacore software. As the dissociation step of SPR signal is very low, close to a weak negative linear drift, the uncertainty on the k_{off} is important and so the k_{on} value is also not reliable. We then apply a local fitting of the association phase allowing the extraction of an observed association phase rate constant, k_{obs}. In such a case, k_{obs} is determined for series of analyte concentrations by fitting the kinetic time course for each concentration C ($k_{\mathrm{obs}} = k_{\mathrm{on}} \times C + k_{\mathrm{off}}$). A plot of k_{obs} *vs* C gives a straight line with slope k_{on} and intercept k_{off} (Figure S16, ESI). The concentration range of the trials used to extract k_{obs} must comply with the following condition: the product $k_{\mathrm{on}} \times C$ must not be negligible compared to k_{off} otherwise the extracted kon is much more inaccurate. After the fitting of the association phase of the response curves and plotted k_{obs} vs C (Figure S16, ESI), the kinetic constants can be determined and the thermodynamic dissociation constant K_D calculated ($K_D=k_{off}/k_{on}$), (Figure 5, Table S2, ESI).

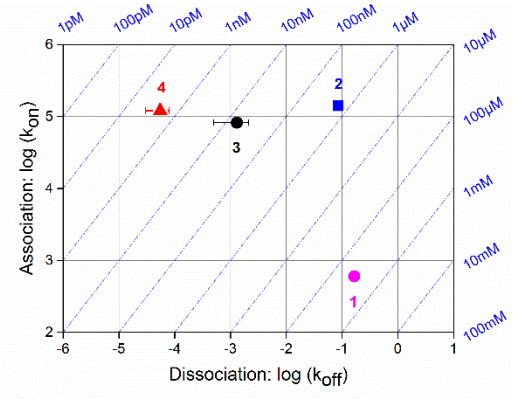

Figure 5. Isoaffinity graph for Fc-containing scaffolds.

The same order of magnitude was obtained for the thermodynamic constant whatever the methods used, steady state or the kinetic fitting. In all the cases, the increase in valency results in an increase of the avidity. Concerning k_{on} and k_{off} values, for the bivalent molecule, the association rate was improved by a factor around 250 compared to monovalent one (respectively, $1.4.10^5$ $M^{-1}s^{-1}$ *vs* 600 $M^{-1}s^{-1}$). The dissociation rate was found to be constant around 10^{-1} s^{-1}. We noticed the reverse for higher valencies: a stability of the association rate constant and a decrease of the dissociation rate constant from to 10^{-1} s^{-1} to 5.10^{-5} s^{-1} for compounds **1** and **4**, respectively. Between **2** and **3**, the dissociation rate decreases by a factor 65 ($8.4\ 10^{-2}$ and $1.3\ 10^{-3}$ s^{-1}, respectively) and a factor 30 between compounds **3** and **4**. The multivalency effect impacts mainly the rate of dissociation as usually reported.[29,33] Similar observations were made by Huskens *et al.* using dynamic force spectroscopy. They studied the kinetic off-rates of multivalent complex formed between di- or trivalent adamantane molecules and β-CD SAM.[34] For the divalent one, the authors reported k_{off} values of 0.2 s^{-1} and 4.10^{-3} s^{-1} for the trivalent one. These values are of the same order of magnitude than those of multivalent Fc measured in the present work. Nevertheless, we expected slightly higher values for Fc as the binding constant of the single pair is significantly higher for adamantane than for Fc (about ten times lower). Such discrepancies could be ascribed to the high flexibility of the adamantyl-functionalized calix[4]arene, which could impact the dissociation rate.

The residence time defined as the average time that a ligand stays bound to its receptor (calculated by $1/k_{off}$) or the half-life of the complex ($Ln2/k_{off}$) provides also useful measurements of binding kinetics. The calculation shows that the half-life was multiplied per 2 from 1 to 2 Fc, per 65 from 2 to 3 Fc and 2400 from 3 to 4 Fc (Table S2, ESI). It results that a valency of 4 ensures a highly stable complexation which could be applied to the irreversible capture of a biomolecule to a surface by Fc/CD interaction. For instance, immobilization of RGD-containing guest molecules was carried out on β-CD SAM for studying the capture of tumor cells.[9,10]

CONCLUSION

In summary, we analyzed the influence of the guest valency from one to four Fc on the stability of the β-CD/Fc inclusion complexes by using surface sensitive techniques. It results that a valency of four ensures a highly stable complexation, which could be applied to the irreversible capture of a biomolecule to an interface. Considering that the sequential binding events are equal and independent, we applied the multivalent model developed by Huskens *at al.*[31] to extract intrinsic binding constants $K_{i,s}$ and effective concentrations of β-CD host. The lower value of $K_{i,s}$ corresponding to an individual host-guest interaction onto a surface compared to $K_{i,l}$ in solution was evidenced by a slight negative cooperativity. This observation has been ascribed to the rigidity of the guest-containing scaffold which can impede the binding of the second, third or fourth guest following the first guest binding. Furthermore, we demonstrated that the rigidity of the cyclodecapeptide scaffold limits significantly the non-specific interactions on β-CD covered surface unlike the flexible polylysine dendrimer. It is worth noting that to our knowledge this feature was not described before. By adapting the corresponding domain on the scaffold, the multimeric Fc-containing scaffold may be conceptually exploited for a wide range of biological applications. The surface modification strategy could be applied to the functionalization of gold nanoparticles for the immobilization of RGD ligands.

Experimental Section

Synthesis of compounds 1, **2**, **3**, **4** and **6**. Compounds **1** to **4** and **6** were synthesized according to previously reported procedures.[9,25] Compounds **1** to **4** were obtained by condensing suitable alkyne peptide derivatives with 1, 2, 3 or 4 ferrocenyl azido fragments Fc-EG4-N3, which was prepared as previously described (Figures S17-S24, ESI.[9,25] Compound **6** was obtained by condensing suitable alkyne peptide derivative with 4 commercially available pegylated derivatives N3-EG4-OH (Figures S25-S26, ESI).

Synthesis of compound 5. Compound 5 was synthesized according to previously reported procedure.[25] Suitable alkyne peptide derivative was coupled to commercially available pegylated derivative HOOC-EG8-NHBoc followed by Boc removal then condensed with 4 ferrocenyl azido fragments Fc-EG4-N3 (Figures S27-S28, ESI).

Synthesis of β-CD thiol (HS-(CH2)11-EG6-CONH-CD). β-CD thiol was synthesized according to previously reported procedure.[35] The synthesis was carried out by condensation of 6-monodeoxy-6-monoamino-β-cyclodextrin on commercially available HS-C11H22-EG6-COONHS in the presence of DIPEA (pH 8–9) in DMF.

Solutions. All aqueous solutions were prepared with ultrapure water (Purelab UHQ Elga). Tris buffer (10 mM Trizma base, 150 mM NaCl, pH 7.4) was used as buffer in QCM-D. In the case of SPR experiments, 0.05% of Tween 20 was added to the Tris buffer. 1mM thiol solutions of HS-(CH2)11-EG4-OH and HS-(CH2)11-EG6-CD were prepared in absolute ethanol.

Surface functionalization. Prior to use, the gold surfaces(QCM-D and SPR sensors) were exposed to a UV-ozone treatment for 10 min using a UV-ozone cleaner (Jelight Company, Irvine, CA, USA). The surfaces were then immersed overnight in a 1 mM ethanolic solution of thiols HS-$(CH_2)_{11}$-EG_4-OH/HS-$(CH_2)_{11}$-EG_6-CONH-CD (hydroxyl-thiol/CD thiol) containing various ratio of thiols, and then carefully rinsed with ethanol and dried under nitrogen**.**

Contact angle measurements: Static contact angles were measured with Milli-Q water using OCA35 Dataphysicis instrument equipped with a CCD camera. Contact angle measurements were performed directly on β-CD SAMs adsorbed on gold coated quartz crystal from the droplet (2 µL) shape analysis software SCA20. The contact angles were evaluated from the average of at least five measurements with droplets being positioned on different places on the surface.

Quartz crystal microbalance with dissipation monitoring (QCM-D). QCM-D measurements were performed using Q-Sense E1 or E4 instruments (Biolin Scientific Västra Frölunda, Sweden) equipped with one or four flow modules, respectively. QCM-D sensors with 100 nm gold-coating (QSX301) were purchased from Biolin Scientific. Besides measurement of bound mass (including trapped solvent), which is provided from changes in the resonance frequency, *f*, of the sensor crystal, the QCM-D technique also provides structural information of biomolecular films via changes in the energy dissipation, *D*, of the sensor crystal. *f* and *D* were measured at the fundamental resonance frequency (4.95 MHz) as well as at the third, fifth, seventh, ninth, eleventh, and thirteenth overtones (n = 3, 5, 7, 9, 11 and 13). Normalized frequency shifts $\Delta f = \Delta f_n/n$ and dissipation shifts $\Delta D = \Delta D_n$ of the seventh overtone are presented unless otherwise stated. Any other overtone would have provided comparable information.

Experiments were conducted in a continuous flow of buffer with a flow rate of 10 µL.min^{-1} by using a peristaltic pump (ISM935C, Ismatec, Switzerland). The temperature of the E1-E4 QCM-D platform and all solutions were stabilized to ensure stable operation at 24°C. All buffers were previously degassed in order to avoid bubble formation in the fluidic system.

In the case of homogeneous, quasi-rigid films (for which $\Delta D/-\Delta f << 4 \times 10^{-7}$ Hz^{-1} for a 5 MHz sensor), the frequency shifts are proportional to the mass uptake per unit area (m_{QCM-D}), which can be deduced from the Sauerbrey relationship:[36]

$$m_{QCM-D} = - C \Delta f \qquad (5)$$

where the mass sensitivity, *C*, is equal to 18 ng.cm^{-2}.Hz^{-1} at f_1 = 4.95 MHz. It should be kept in mind that if the film is solvated, the acoustic areal mass density of the film will be composed of the areal mass densities of the adsorbate, m_{ads}, and the hydrodynamically coupled solvent, $m_{solvent}$:

$$m_{QCM-D} = m_{ads} + m_{solvent} \qquad (6)$$

Electrochemistry. Electrochemical measurements were performed using electrochemical QCM-D modules (Biolin Scientific), connected with a CHI 440 potentiostat (CH-Instruments, Inc., USA). Electrode potentials were referred to Ag/AgCl/KCl (3 M). The counter electrode was platinum and the working electrode was the functionalized gold-coated QCM-D sensor. For electrolysis experiments, electrochemical cells of 10 mL were used, the working electrode is a large glassy carbon electrode of 1.2 cm^2, the counter electrode is a platinum wire. Cyclic voltammograms were recorded on glassy carbon electrode (CH-Instruments) diam. 3 mm. Prior to use, GC electrodes were polished with alumina slurries(1 µm then 0.05 µm particle size), rinsed with Milli-Q water and dried using N_2.

SPR Measurements. All SPR measurements were performed at 25°C in a four flow-cell Biacore T200 instrument (GE Healthcare) where the four flow cells were used as sample channel as the gold sensor chip was uniformly covered with β-CD SAM.

After the functionalization with the β-CD SAM, the gold sensor chip was mounted inside the instrument and incubated in the running buffer (Tris buffer 10 mM, 150 mM NaCl pH 7.4 and 0.05% Tween 20). The guest molecules solutions were injected successively for a maximum of 420s at a flow rate 50 µL.min^{-1} at concentrations of 10, 25, 50, 75, 100, 125, 150, 200, 300, 400, 500, 600, 700 and 1000 µM. Each guest molecule injection was followed by a 600s running buffer rinsing step, and a regeneration step (30s) using a fresh solution of 0.5 mM oxidized ferrocenylmethanol (Fc-OH) solution (Figure S29, ESI).

The binding rate constants of Fc-containing scaffolds/β-CD SAM interactions were calculated by a non-linear fitting of the association phase, the experimental curves were fitted using a 1:1 model to obtain the kinetic rate constant k_{obs}. The k_{obs} parameter depends on the kinetic association rate k_{on} and dissociation rate k_{off}:

$$k_{obs} = k_{on}.C + k_{off} \qquad (7)$$

where C is the concentration of the analyte in the flow cell. The plot of k_{obs} versus C allows the determination of the two kinetic constants: k_{on} the slope of the curve and k_{off} the intercept. The reported values are obtained from the average of representative independent experiments, and the errors provided are standard deviations from the mean. Each experiment was repeated at least three times.

Acknowledgements

This work was partially supported by the French National Agency (ANR) under ECSTASE, Contract ANR-10-blan-1517, (Rational design of a sensitive and enantiospecific electrocatalytically-amplified aptasensor for amphetamine derivatives drugs), under ARCANE and CBH-EUR-GS (ANR-17-EURE-0003) and the University Grenoble Alpes. The authors wish to acknowledge the support from the ICMG (FR2607) Chemistry Nanobio Platform, Grenoble. Prof. P. Labbé is acknowledged for fruitful discussions and E. Laigre for the drawing of the graphical abstract.

Keywords: multivalency • cyclodextrin • ferrocene • SAM surface • host-guest interaction

[1] X. Ma, Y. Zhao, *Chem. Rev.* **2015**, *115*, 7794-7839.
[2] C. B. Rodell, J. E. Mealy, J. A. Burdick, *Bioconjugate Chem.* **2015**, *26*, 2279.
[3] M. Pagel, R. Hassert, T. John, K. Braun, M. Wieβler, B. Abel, A.G. Beck-Sickinger, *Angew. Chem. Int. Ed.* **2016**, *55*, 4826-4830.
[4] J. Boekhoven, C. M. Rubert Pérez, S. Sur, A. Worthy, S. I. Stupp, *Angew. Chem. Int. Ed.* **2013**, *52*, 12077-12080.
[5] Y. Ma, X. Tian, L. Liu, J. Pan, G. Pan, *Acc. Chem. Res.* **2019**, *52*, 1611-1622.
[6] Q. An, J. Brinkmann, J. Huskens, S. Krabbenborg, J. de Boer, P. Jonkheijm, *Angew. Chem. Int. Ed.* **2012**, *51*, 12233-12237.
[7] L. Yang, A. Gomez-Casado, J.F. Young, H.D. Nguyen, J. Cabanas-Danès, J. Huskens, L. Brunsveld, P. Jonkheijm, *J. Am. Chem. Soc* **2012**, *134*, 19199-19206.
[8] D.H. Schwartz, W.A.M. Elgaher, K. Hollemeyer, A.K.H. Hirsch, G. Wenz *J. Mater. Chem. B* **2019**, *7*, 6148-6155.
[9] M. Degardin, D. Thakar, M. Claron, R. P. Richter, L. Coche-Guérente, D. Boturyn, *J. Mat. Chem. B* **2017**, *5*, 4745-4753.
[10] D. Thakar, L. Coche-Guerente, M. Claron, C. H. F. Wenk, J. Dejeu, P. Dumy, P. Labbé, D. Boturyn, *ChemBioChem* **2014**, *15*, 377-381.
[11] R. Castro, I. Cuadrado, B. Alonso, C. M. Casado, M. Moran, A. E. Kaifer, *J. Am. Chem. Soc.* **1997**, *119*, 5760 -5761.
[12] D. Boturyn, E. Defrancq, G. T. Dolphin, J. Garcia, P. Labbe, O. Renaudet, P. Dumy. *J. Pept. Sci.* **2008**, *14*, 224-240.
[13] J. D. Badjicä, A. Nelson, S. J. Cantrill, W. B. Turnbull, J. F. Stoddart, *Acc. Chem. Res.* **2005**, *38*, 723-732.
[14] J. Huskens, *Curr. Opin. Chem. Biol.* **2006**, *10*, 537-543.
[15] C. A. Nijhuis, J. Huskens, D. N. Reinhoudt, *J. Am. Chem. Soc.* **2004**, *126*, 12266-12267.
[16] C. Fasting, C. A. Schalley, M. Weber, O. Seitz, S. Hecht, B. Koksch, J. Dernedde, C. Graf, E.-W. Knapp, R. Haag, *Angew. Chem. Int. Ed.* **2012**, *51*, 10472–10498.
[17] L. Röglin, E. H. M. Lempens, E. W. Meijer, *Angew. Chem. Int. Ed.* **2011**, *50*, 102 – 112.
[18] G.V. Dubacheva, A. Van Der Heyden, P. Dumy, O. Kaftan, R. Auzely-Velty, L. Coche-Guérente, P. Labbé, *Langmuir* **2010**, *26*, 13976-13986.
[19] G.V. Dubacheva, P. Dumy, R. Auzely-Velty, P. Schaaf, F. Boulmedais, L. Jierry, L. Coche-Guérente, P. Labbé, *Soft Matter* **2010**, *6*, 3747-3750.
[20] G. V. D Dubacheva, M. Galibert, L. Coche-Guérente, P. Dumy, D. Boturyn, P. Labbé, *Chem Commun.* **2011**, *47*(12), 3565-3567.
[21] M.T. Rojas, R. Königer, J.F. Stoddart, A.E. Kaifer, J. *Am. Chem. Soc.* **1995**, *117*, 336-343.
[22] G. Nelles, M. Weisser, R. Bach, P. Wohlfart, G. Wenz, S. Mittler-Neher *J. Am. Chem. Soc.* **1996**, *118*, 5039-5046.
[23] M.W.J. Beulen, J. Bügler, B. Lammerink, F.A.J. Geurts, E.M.E.F. Biemond, K.G.C. van Leerdam, F.C.J.M. van Veggel, J.F.J. Engbersen, D.N. Reinhoudt *Langmuir* **1998**, *14*,6424-6429.
[24] M.R. de Jong, J. Huskens, D.N. Reinhoudt, *Chem. Eur. J.* **2001**, *7*, 4164-417.
[25] E. Garanger, D. Boturyn, J.-L. Coll, M.-C. Favrot, P. Dumy, *Org. Biomol. Chem.* **2006**, *4*, 1958-1965.
[26] S. Peluso, T. Rückle, C. Lehmann, M. Mutter, C. Peggion, M. Crisma, *ChemBioChem* **2001**, *2*, 432-437.
[27] A. Grassin, M. Jourdan, P. Dumy, D. Boturyn, *ChemBioChem* **2016**, *17*, 515-520.
[28] Y. Domi, Yoshinaga, K. Shimazu, M.D. Porter, *Langmuir*, **2009**, *25*, 8094–8100.
[29] M. Mannen, S.K. Choi, G.M. Whitesides, *Angew. Chem. Int. Ed.* **1998**, *37*, 2754-2794.
[30] A. Mudler, T. Auletta, A. Sartori, S. Del Ciotto, A. Casnati, R. Ungaro, J. Huskens, D. N. Reinhoudt, *J. Am. Chem. Soc*, **2004**, *126*, 6627-6636.
[31] J. Huskens, A. Mudler, T. Auletta, C. A. Nijhuis, M. J. W. Ludden, D. N. Reinhoudt, *J. Am. Chem. Soc.* **2004**, *126*, 6784-6797.
[32] D. Boturyn, J.-L. Coll, E. Garanger, M.-C. Favrot, P. Dumy, *J. Am. Chem. Soc.* **2004**, *126*, 5730-5739.
[33] E. Laigre, D. Goyard, C. Tiertant, J. Dejeu, O. Renaudet, *Org. Biomol. Chem.* **2018**, *16*, 8899-8903.
[34] A. Gomez-Casado, H. H. Dam, M. Deniz Yilmaz, D. Florea, P. Jonkheijm, J. Huskens, *J. Am. Chem. Soc.* **2011**, *133*, 10849–10857.
[35] J. Bacharouche, M. Degardin, L. Jierry, C. Carteret, P. Lavalle, J. Hemmerle, B. Senger, R. Auzely-Velty, F. Boulmedais, D. Boturyn, L. Coche-Guerente, P. Schaaf, G. Francius, *J. Mater. Chem. B* **2015**, *3*, 1801-1812.
[36] I. Reviakine, D. Johannsmann, R.P. Richter, *Anal. Chem.* **2011**, *83*, 8838-8848.

Supporting Information

Impact of multimeric ferrocene-containing cyclodecapeptide scaffold on host-guest interactions at a β-cyclodextrin covered surface

E. Sanchez Perez, R. Ritu , P. Bruyat, C. Cepeda, M. Degardin, J. Dejeu, D. Boturyn, L. Coche-Guérente.

Materials supports.

All Fmoc amino acid derivatives and resins were purchased from Advanced ChemTech Europe (Brussels, Belgium), Bachem Biochimie SARL (Voisins-Les-Bretonneux, France) and France Biochem S.A. (Meudon, France). PyBOP was purchased from France Biochem and other reagents were obtained from either Aldrich (Saint Quentin Fallavier, France) or Acros (Noisy-Le-Grand, France). N_3-EG_4-NHS and HOOC-EG_8-NHBoc were purchased from IRIS Biotech GMBH. RP-UHPLC analysis were performed on Waters equipment consisting of a Waters Acquity H-Class Bio UPLC combined to a Waters SQ Detector 2 mass spectrometer. The analytical column used was a ACQUITY UPLC BEH C18 Column, 130 Å, 1.7 µm, 2.1 mm x 50 mm operated at 0.6 $mL.min^{-1}$ with linear gradient programs in 2.20 min run time (routine program: 5% to 100% B in 2.20 min). UV monitoring was performed at 214 nm. Solvent A consisted of H_2O containing 0.1% formic acid (FA) and solvent B consisted of CH_3CN containing 0.1% FA. Water was of Milli-Q quality. CH_3CN and FA were LC-MS grade. RP-HPLC analysis were performed on a Waters system equipped with a Waters 600 controller and a Waters 2487 Dual Absorbance Detector. The purity of peptide derivatives was analyzed on an analytical column (Macherey-Nagel Nucleosil 120 Å 3 µm C18 particles, 30 x 4.6 mm) using the following solvent system: solvent A, water containing 0.09% TFA; solvent B, acetonitrile containing 0.09% TFA and 9.91% H_2O; a flow rate of 1.3 $mL.min^{-1}$ was employed with a linear gradient (5 to 100% B in 20 min). UV absorbances were monitored at 214 nm and 250 nm simultaneously. Preparative column (Delta-Pak™ 100 Å 15 µm C18 particles, 200 x 2.5 mm) were used to purify the crude peptides (when necessary) by using an identical solvent system at a flow rate of 22 $mL.min^{-1}$. RP-HPLC purifications were either performed on Gilson GX-281 (high quantities: hundred of mg) or GX-271 equipment (low quantities: few mg). For GX-281, the preparative column, Macherey-Nagel 100 Å 7 µm C18 particles, 250 x 21 mm was operated at 20.84 $mL.min^{-1}$. For GX-271, the preparative column, Macherey-Nagel 300 Å 7 µm C18 particles, 250 x 10 mm (Hoerdt, France) was operated at 4.65 $mL.min^{-1}$. Linear gradient programs in 30 min run time were used and solvents A and B were the same as the ones used in RP-HPLC analysis. Electron spray ionization mass spectra (ESI-MS) were recorded on an Esquire 3000 (Bruker) spectrometer. The analyses were performed in positive mode for peptide derivatives using 50% aqueous acetonitrile as eluent. The multiply charged data produced by the mass spectrometer on the m/z scale were converted to the molecular weight. Tris(hydroxymethyl)aminomethane (Tris), (11-Mercaptoundecyl)tetra(ethylene glycol) (HS-$(CH_2)_{11}$-EG_4-OH) and NaCl were purchased from Sigma-Aldrich (Saint Quentin Fallavier, France). Polyoxyethelene sorbitan monolaurate (Tween ®20) was purchased from Euromedex, ethanol grade for analysis was purchased from Acros (Noisy-Le-Grand, France), 6-monodeoxy-6-monoamino-β-cyclodextrin was provided by AraChem (The Nerderlands), 2-hydroxypropyl-β-Cyclodextrin, ferrocenylmethanol and potassium octacynaomolybdate were purchased from Sigma-Aldrich (Saint Quentin Fallavier, France). HS-$C_{11}H_{22}$-EG_6-COONHS was purchased from Prochimia Surfaces (ProChimia Surfaces, Sopot, Poland).

Additional figures:

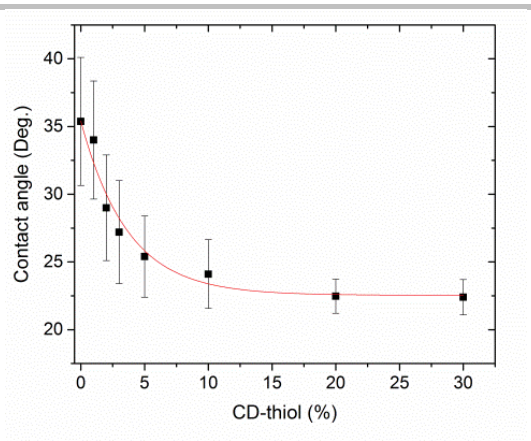

Figgure S1. Contact angle of water on β-CD SAMs as a function of the molar ratios of CD-thiol in the solution used to prepare the β-CD SAMs.

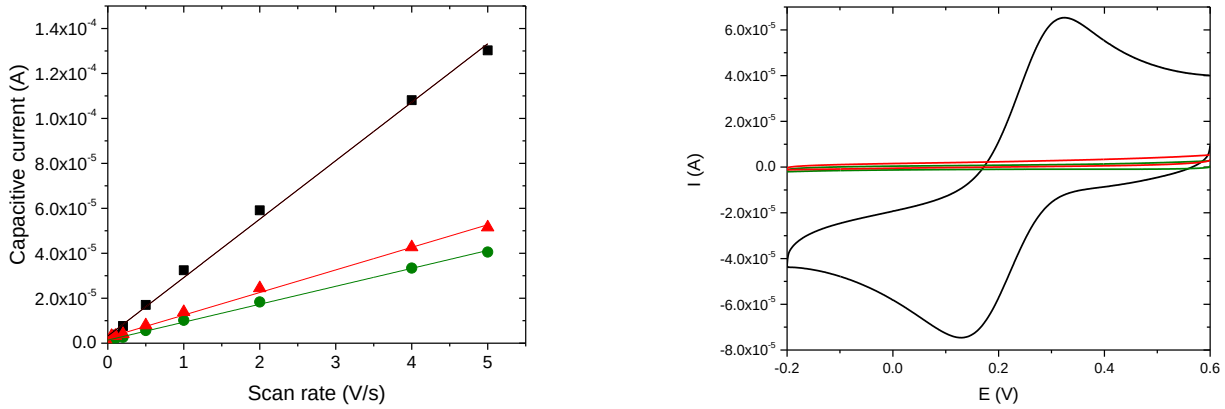

A B

Figure S2. (A) Plots of capacitive current, measured at 0.1V on cyclic voltammograms in 0,2 M aqueous solution of Na_2SO_4 on bare gold surface (black square), Hydroxyl-SAM (green disk) and β-CD SAM (prepared from 20% molar ratio of β-CD thiol) (red triangle). (B) Cyclic voltammograms of $Fe(CN)_6^{3-}$ 0,4 mM, 0.2M Na_2SO_4 solution, black curve: on bare gold, green curve: hydroxyl-SAM and red curve: β-CD SAM (scan rate: 0.1 V/s).

The capacitive current is the product of the scan rate, double layer capacitance and electrode surface area. The linear fitting of the data plots (Fig. S2A) provides the following slopes:

- On bare gold: 2.6E-5 $A.s.V^{-1}$
- On Hydroxyl-SAM: 1.4E-6 $A.s.V^{-1}$
- On β-CD SAM: 2.5E-6 $A.s.V^{-1}$

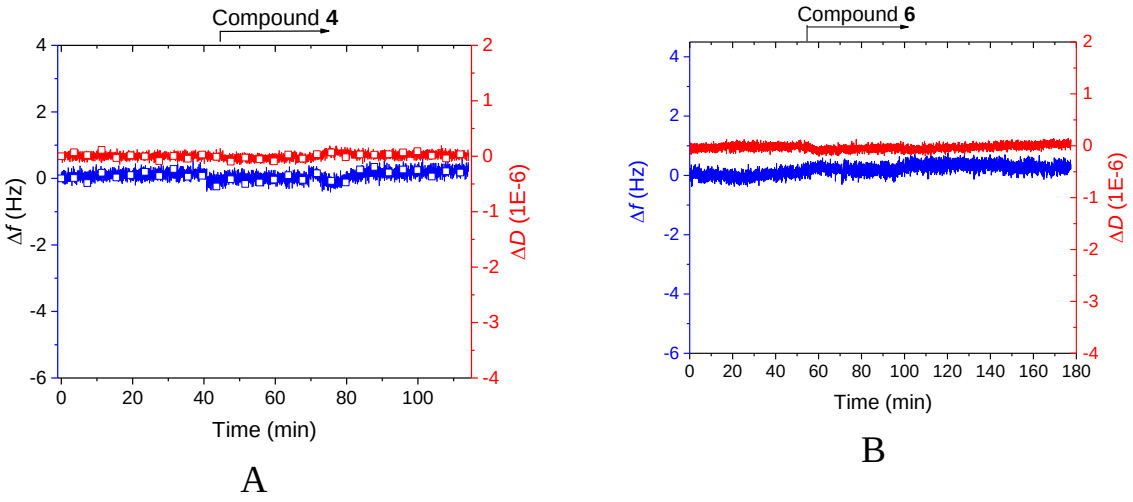

Figure S3. QCM-D signals (resonant frequency – blue, dissipation– red) recorded during the injection of 5 µM of (A) Fc-containing compound **4** on hydroxyl-SAM prepared from 100% of hydroxyl-thiol; (B) cyclodecapeptide **6** without guest motifs. The arrows represent the start and duration of sample injections. T = 24°C, flow rate = 10 µL.min^{-1}.

The QCM-D profile of figure S3B shows the absence of non-specific adsorption of compound **4**.

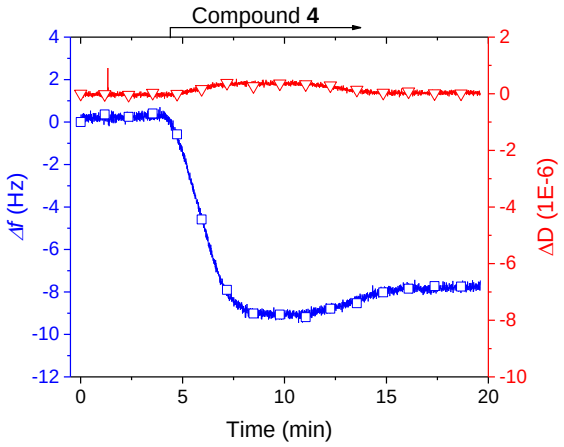

Figure S4. QCM-D signals (resonant frequency – blue, dissipation– red) recorded during the injection of 5 µM Fc-containing compound **4** on β-CD SAM prepared from the covalent grafting of β-CD on azide-SAM (25% of thiol azide) by CuAAC. The arrow represents the start and duration of sample injection. T = 24°C, flow rate = 10 µL.min^{-1}. An average of hydrated mass of 150 ± 30ng/cm^2 was calculated from the shift in frequency recorded after rinsing with the buffer.

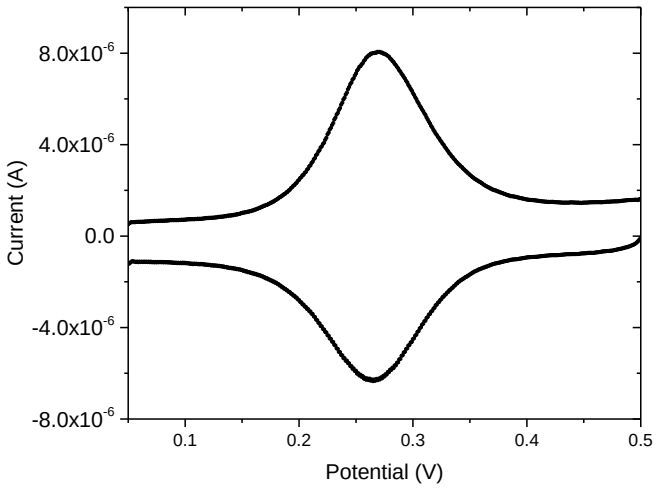

Fig. S5: Cyclic voltammogramm of compound **4** trapped in the host cavities of β-CD SAM adsorbed on a gold quartz crystal (Φ 1 cm) recorded in an aqueous solution of 0.1M of KPF_6 after an incubation of 15 min of a 5µM solution of **4** in Tris buffer and a rinsing steps.

Calculation of Fc surface density by using Faraday law:

Surface concentrations of Fc were determined from Faraday's law from the charge associated with the oxidation voltammetric peak Q_a.

$$\Gamma_{Fc} = \frac{Q_a}{zFA} \qquad (1)$$

With z = 1 (number of exchange electron by Fc during the oxidation step), F = 96485 C. mol^{-1} and A is the area of gold surface (quartz crystal).

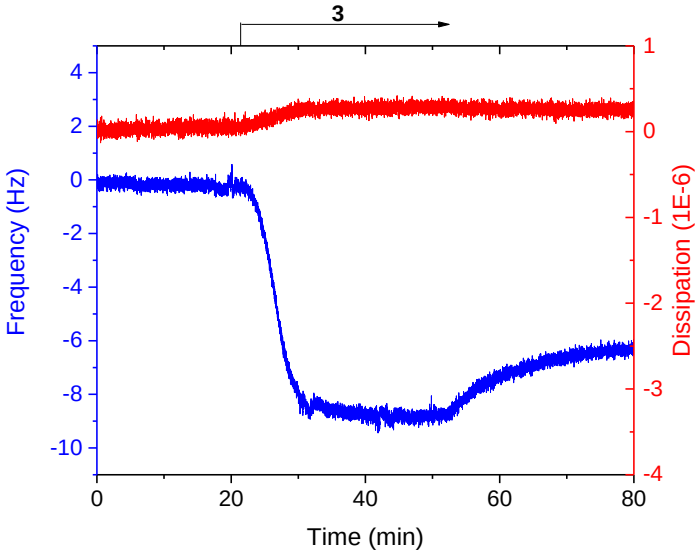

Figure S6. QCM-D profile characterizing the adsorption of compound **3** (5µM) to β-CD SAM surface.

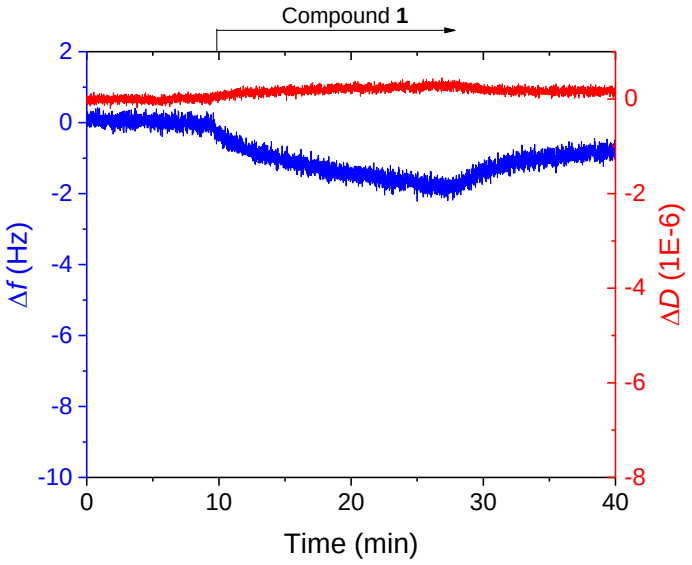

Figure S7. QCM-D profile characterizing the adsorption of compound **1** (50µM) to β-CD SAM surface.

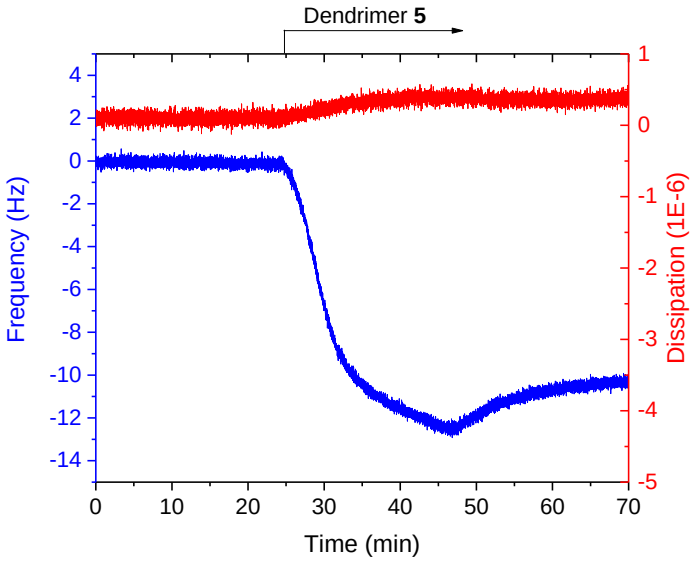

Figure S8. QCM-D profile characterizing the adsorption of dendrimer **5** (5µM) to β-CD SAM surface.

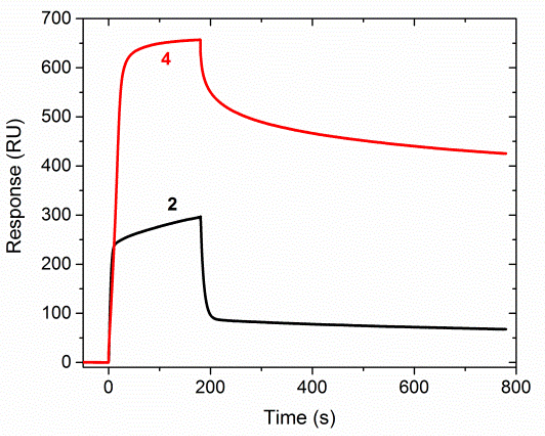

Figure S9: SPR sensorgrams characterizing the binding of compounds **2** (black curve) and **4** (red curve) on β-CD SAM surface.

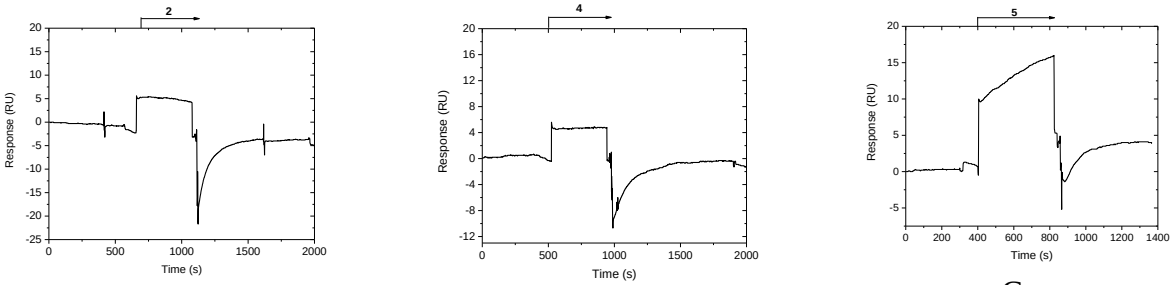

Figure S10. SPR sensorgram of 200 nM compounds **2** (A), **4** (B), **5** (C) on hydroxy-SAM (prepared from a pure hydroxyl thiol solution).

Figure S10 depicted the responses of Fc-containing compounds on hydroxyl-SAM, the sensorgrams came from manual run recording. It shows the reversibility of the adsorption of compounds **2** and **4** on hydroxyl-SAM, indeed the signals recovered the baseline level upon rinsing with buffer confirming the reversibility of the interaction. The magnitude of the signal is mainly due to change of the refractive index from buffer to 1 µM solution. In contrast, for dendrimer **5** during the contact time of the sensor chip with the analyte the SPR signal did not show a plateau but a continuous positive drift and after the rinsing step the

magnitude of the signal appears higher than the initial baseline which reflecting an irreversible adsorption of **5** on hydroxyl-SAM.

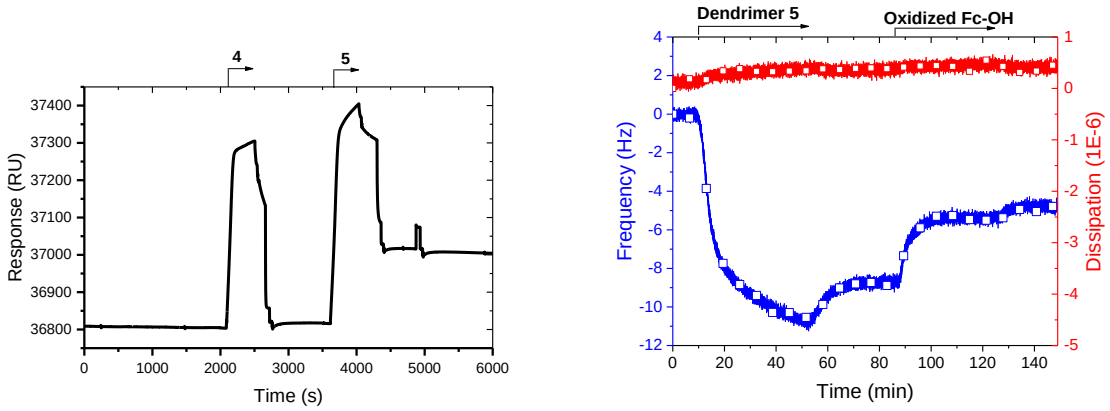

A B

Figure S11: Graphs illustrating the inefficient dissociation of the inclusion complex **5**/β-CD SAM by using 0.5 mM Fc^{+}-OH solution (A) SPR sensorgram of compounds **4** and **5**. (B) QCM-D profile of the adsorption of dendrimer 5 and its partial desorption by using a 0.5 mM solution of Fc^{+}-OH. The regeneration step is efficient for the compounds **4** while it appears inefficient for **5**.

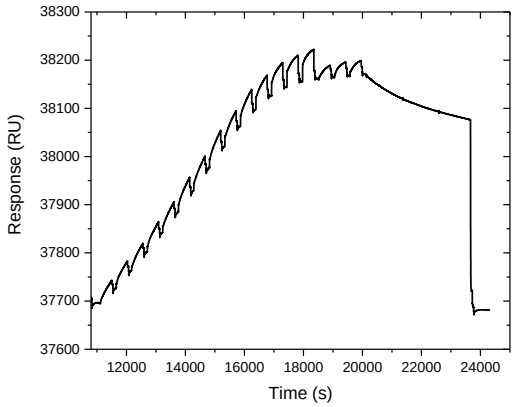

Figure S12. Successive injections of 5 nM compound **4** under manual run (flow rate: 50 µL/min).

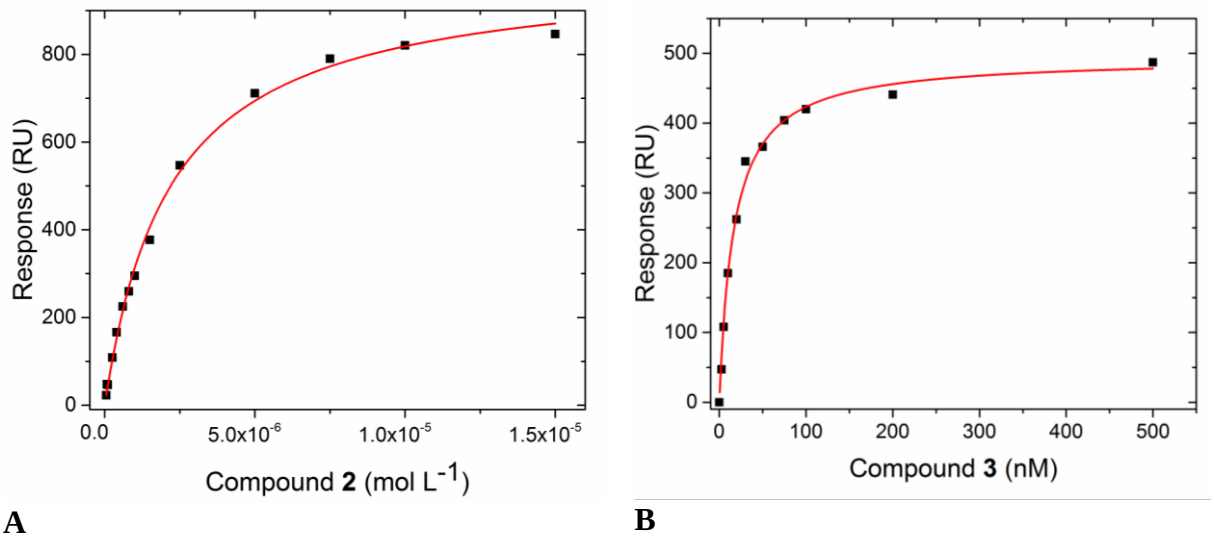

A **B**

Figure S13. Langmuir isotherms for the binding of compounds **2** (A) and **3** (B).

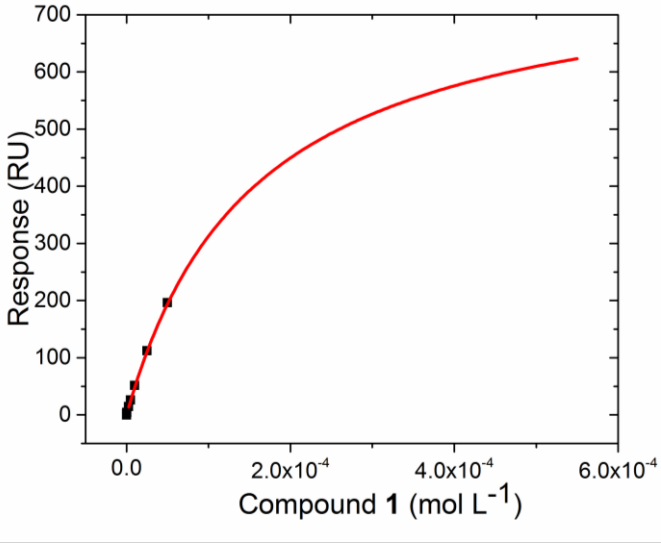

Figure S14. Langmuir binding isotherm for compound **1** plotted (squares represent the experimental points of the sensorgrams at steady-state equilibrium), the red curve correspond the fitted curve providing a R_{max} of 800 RU and a K_D of 160 µM.

Quantitative characterization of multivalency

Free energy of binding: $\Delta G° = -RT\,Ln K_A$ (1)

with K_A is the equilibrium association rate constant ($1/K_D$).

For characterizing the polyvalent interactions, Whitesides et al. defined a degree of cooperativity α factor.[1]

$$\propto = \frac{\Delta G_{avg}^{poly}}{\Delta G^{mono}} \quad (2)$$

ΔG_{avg}^{poly} is the average free of interaction between a single ligand moiety and a single receptor moiety in the polyvalent interaction, $\left(\Delta G_{avg}^{poly} = \frac{\Delta G_n^{poly}}{n}\right)$, ΔG_n^{poly} refers to the global interaction and n is the number of ligands.

Table S1: Calculation of $K_{i,s}$ using the equation (3) and values of $C_{eff,max}$ = 0.387 M calculated with a linker length of 2.85 nm and $C_{eff,max}$ = 0.567M calculated with a linker length of 1.38 nm (1.38 nm representing the minimum and 2.85 nm the maximum distances between two RGD determined by molecular dynamics): [3]

$$K_{i,s} = \left(\frac{K_A}{(C_{eff,max})^{(n-1)}}\right)^{1/n} \quad (3)$$

Compound	K_A [a]	$K_{i,s}$ (min-max)
1	7700	/
2	$4.6\ 10^5$	900-1090 M^{-1}

3	6.7 10^7	593-765 M^{-1}
4	1.0 10^9	272-362 M^{-1}

[a]: $K_A = 1/K_D$ is the overall binding constant, obtained by using a Langmuir model, K_A (M^{-1})

Application of Huskens' multivalency model to Fc/CD-SAM interaction.[2]

The multivalent model described by Huskens et al. that allows quantifying the binding of multivalent ligands to a surface covered with closely packed receptors was applied to the present host-guest system.[2] The SPR responses were fitted according to eq. (4)

$$R\ (RU) = \frac{[Guest]_s}{[CD_s]_{tot}} \frac{R_{max}}{p_{av}} \qquad (4)$$

Where R is the SPR response measured on the sensorgram plateau for various guest concentrations, $[Guest]_s$ is the total guest concentration on the surface including the binding of monovalent, divalent, trivalent or tetravalent Fc-CD (depending on the valency n of the Fc-containing scaffold), $[CD_s]_{tot}$ is total concentration in CD on the β-CD SAM platform, R_{max} corresponds to the maximal SPR response expected for a fully covered surface and p_{av} represents the average number of interactions used by a guest molecule to bind the surface, it is defined by the following equation (5):[2]

$$p_{av} = \frac{[CD_s]_{tot} - [CD_s]}{[Guest]_s} \qquad (5)$$

The concentrations in guest on the surface were expressed as a function of the intrinsic binding constants $K_{i,s}$ and effective concentration C_{eff}. For such development, we adapted to our experimental conditions of study: (i) absence of competitor (β-CD) in solution, (ii) the concentration of free guest in solution was equal to the total guest concentration injected as we made the assumption that in the Biacore microfluidic set-up the concentration of host-guest complexes is negligible compared with the concentration of flowing guest.

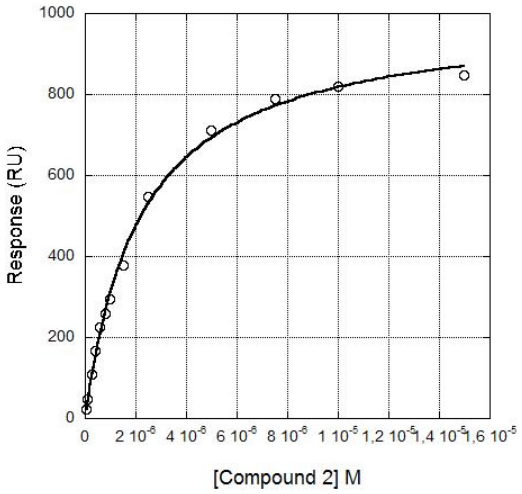

A

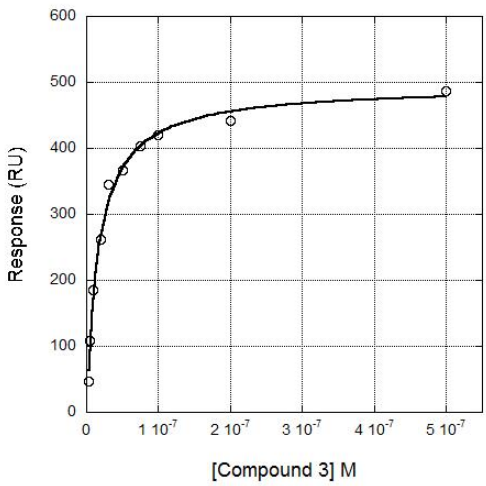

B

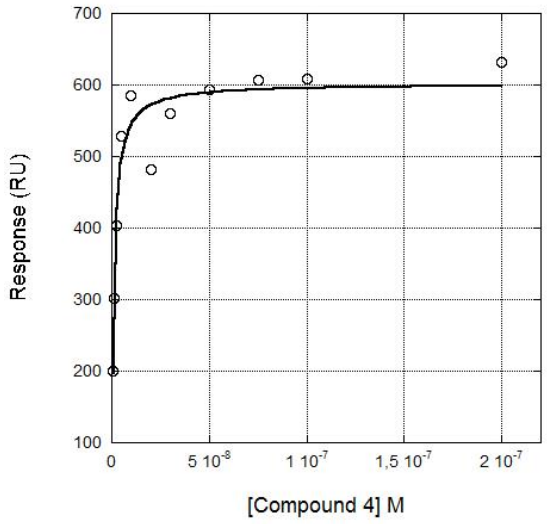

C

Figure S15. SPR analysis of Fc-containing scaffolds **2** (A), **3** (B) and **4** (C) binding on CD-SAM (data points) and fitting for the multivalent model (solid lines).[1]

Table S2: Kinetic and thermodynamic constant determined from the sensorgram.

Guest molecules	Kinetic K_D (nM)	k_{on} (10^5 M^{-1}. S^{-1})	k_{off} (10^{-2} s^{-1})	Time of 50% dissociation rate (s)[a]
1	277 570 ± 19 358	0.060 ± 0.004	16 ± 0.04	4.3
2	614 ± 119	1.40 ± 0.12	8.4 ± 1.0	8.25
3	14 ± 7	0.82 ± 0.12	0.13 ± 0.08	533
4	0.43 ± 0.1	1.3 ± 0.27	0.005 ± 0.0025	$2\ 10^4$

[a]: Off-rates for 50% dissociation (or half-life of the complex) calculated by considering a reaction rate of first order, $Ln2/k_{off}$.

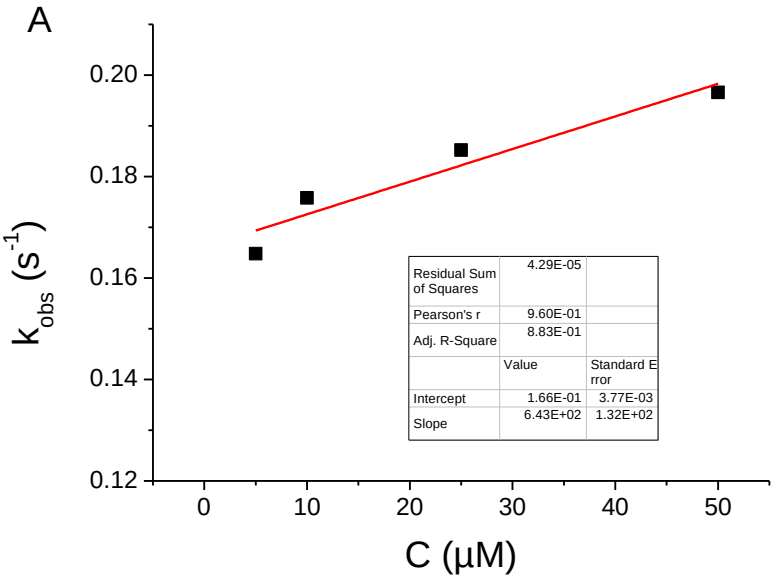

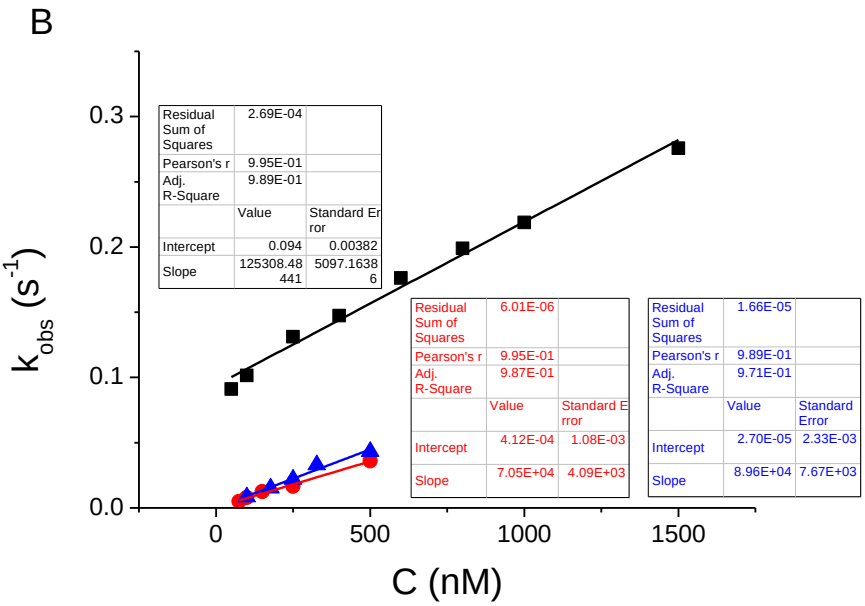

Figure S16. Observed association phase rate constant k_{obs} versus the concentration C of the analyte for compound A) **1** and B) **2** (black), **3** (red) and **4** (blue).

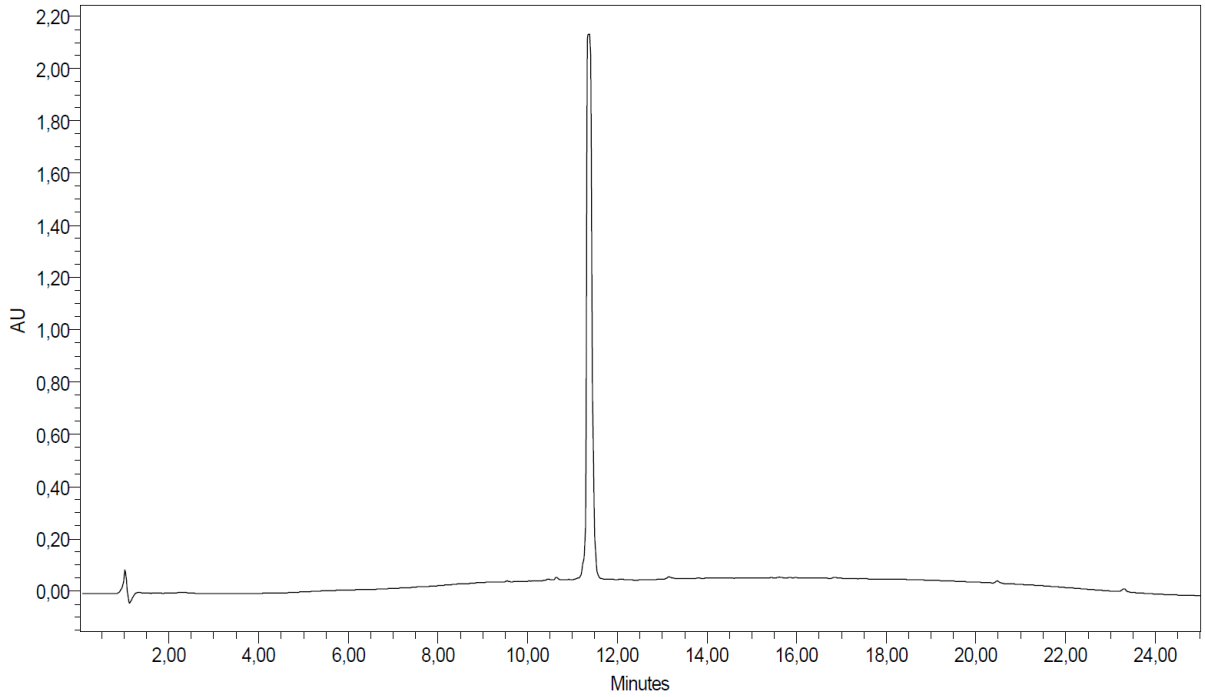

Figure S17: RP-HPLC profile of **1**.

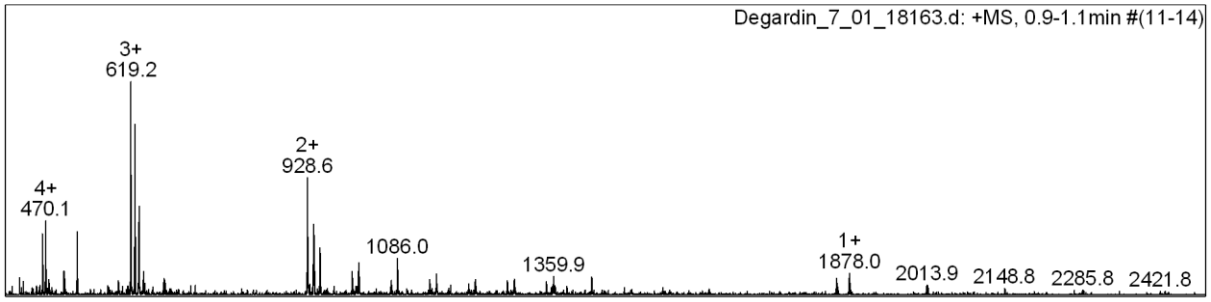

Mass spectrum (ESI, positive mode) calculated mass for $C_{85}H_{139}Fe_1N_{17}O_{25}$: 1855.0; found: 1855.4.
Figure S18. ESI-MS analysis of **1**.

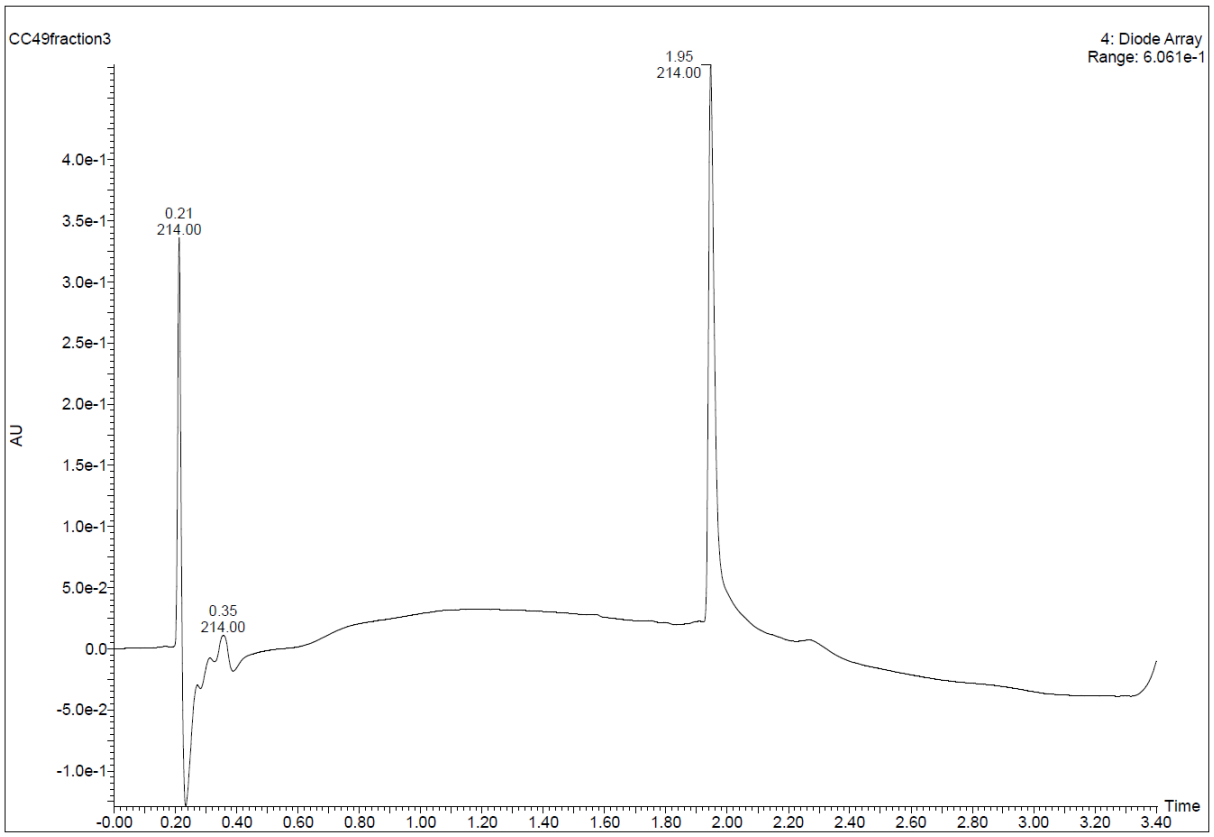

Figure S19. RP-UHPLC profile of **2**.

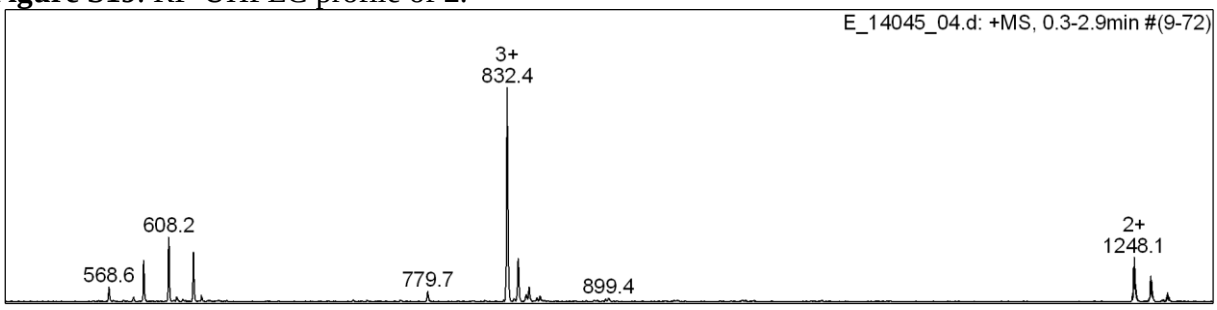

Mass spectrum (ESI, positive mode) calculated mass for $C_{116}H_{184}Fe_2N_{22}O_{31}$: 2493.2; found: 2493.2.
Figure S20. ESI-MS analysis of **2**.

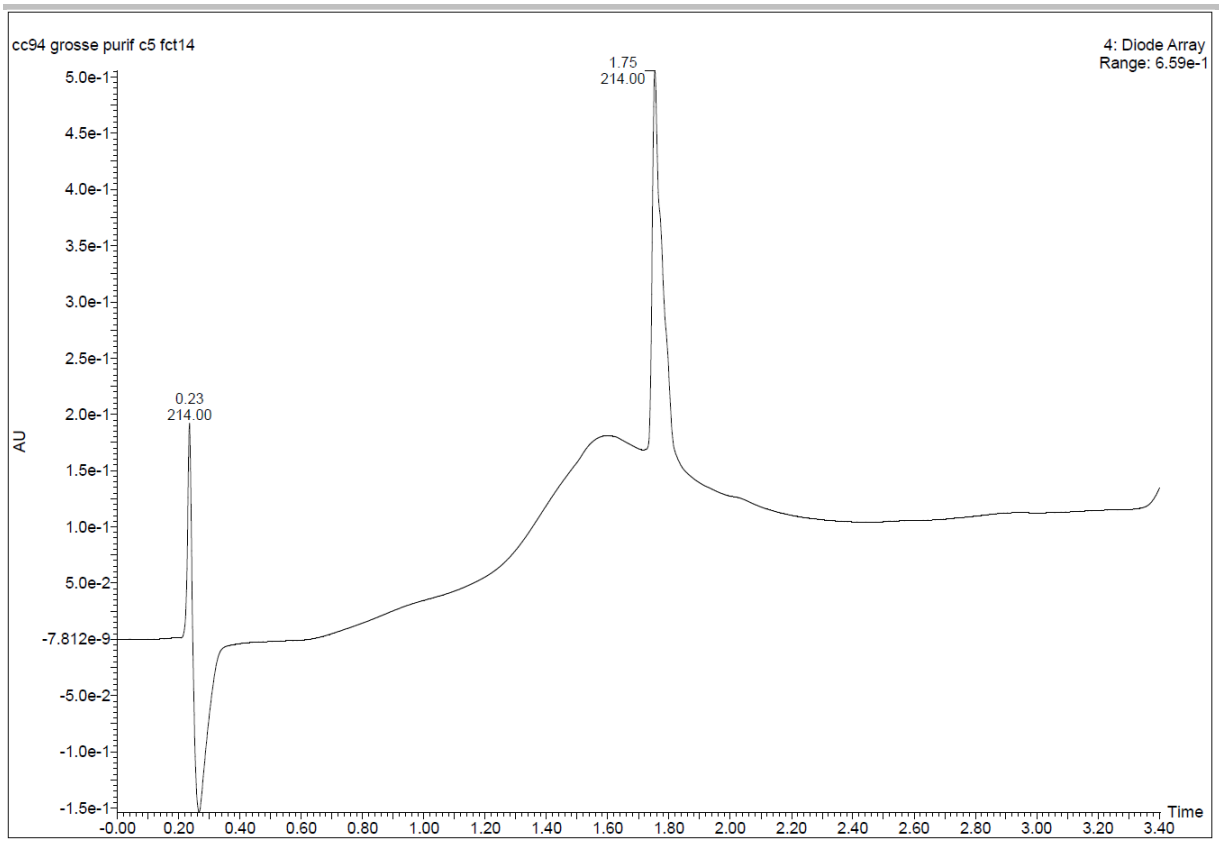

Figure S21. RP-UHPLC profile of **3**.

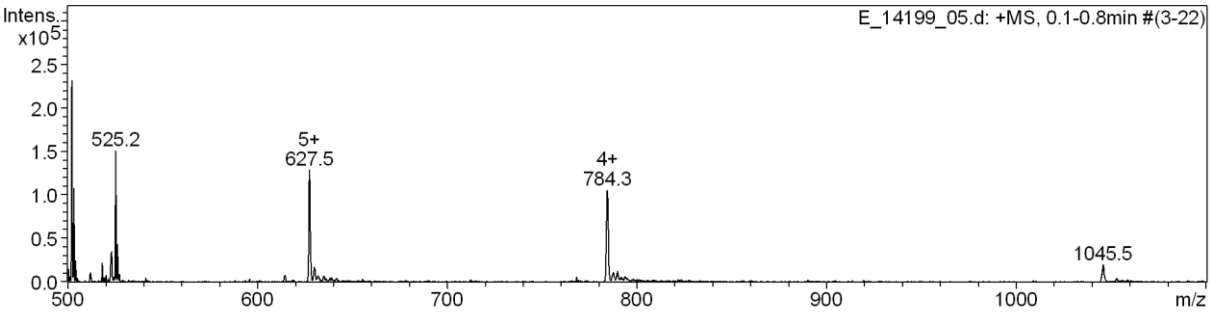

Mass spectrum (ESI, positive mode) calculated mass for $C_{147}H_{229}Fe_3N_{27}O_{37}$: 3133.5; found: 3133.6.
Figure S22. ESI-MS analysis of **3**.

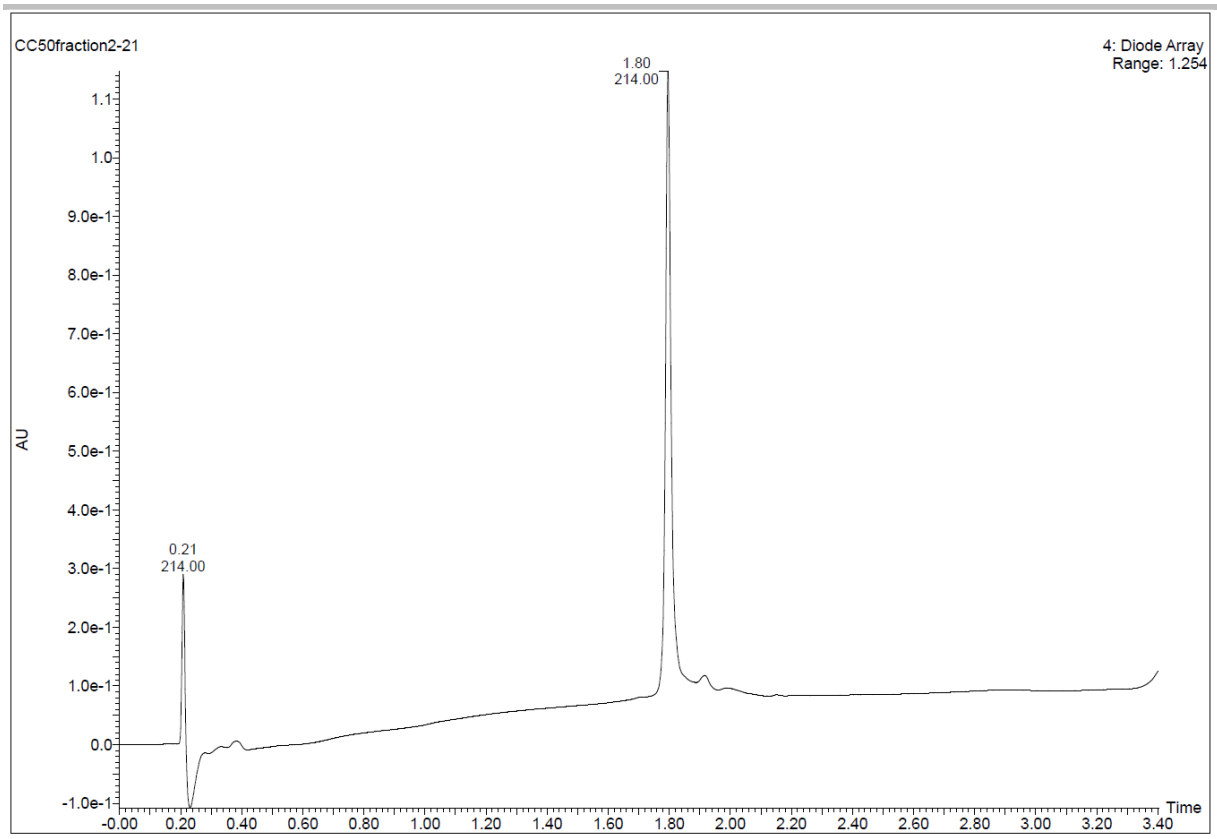

Figure S23. RP-UHPLC profile of **4**.

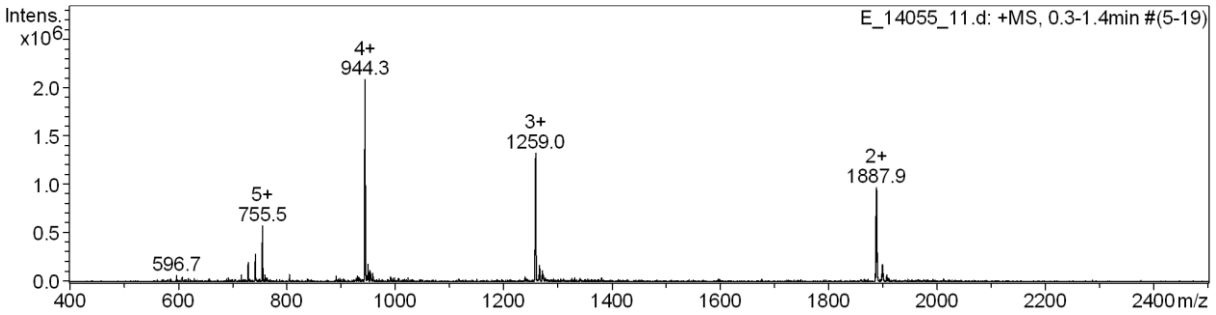

Mass spectrum (ESI, positive mode) calculated mass for $C_{178}H_{274}Fe_4N_{32}O_{43}$: 3773.7; found: 3773.0.
Figure S24. ESI-MS analysis of **4**.

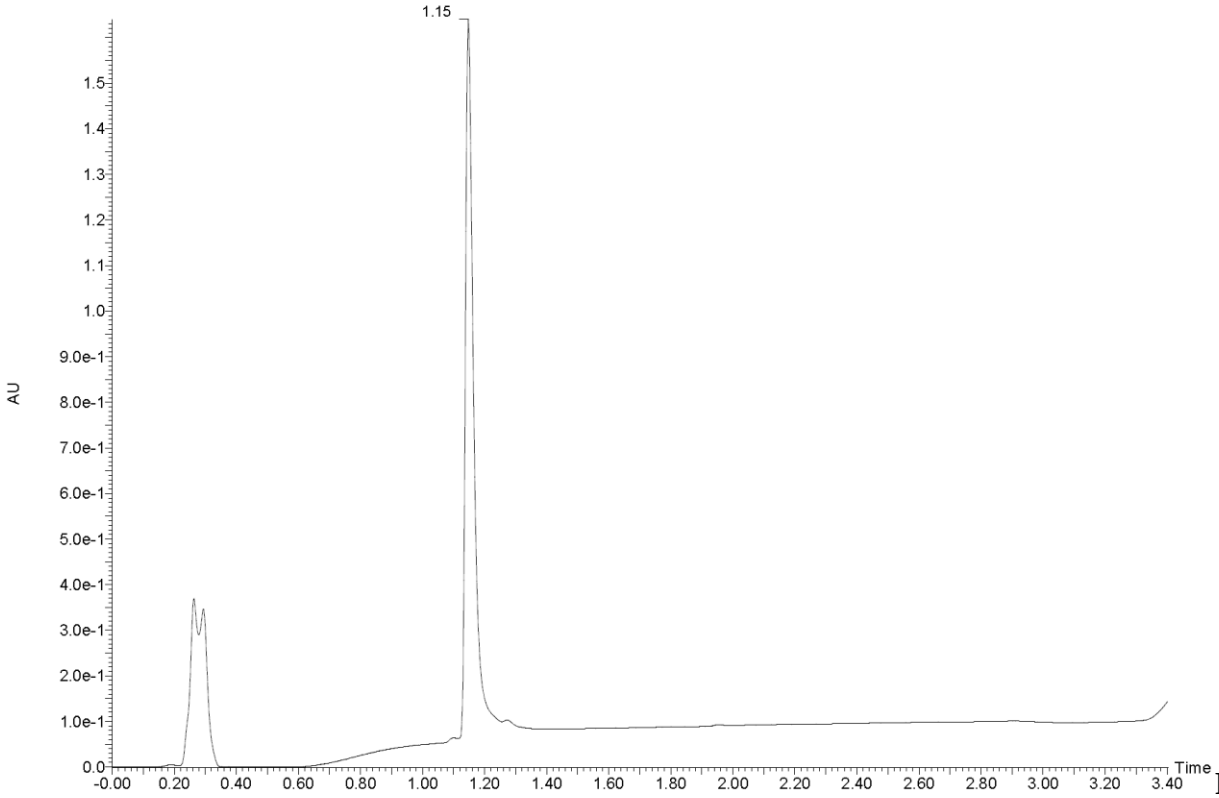

Figure S25. RP-HPLC profile of compound **6**.

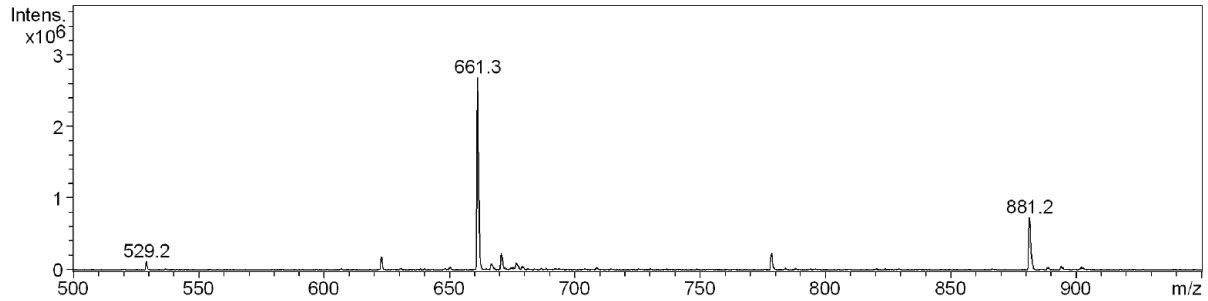

Mass spectrum (ESI, positive mode) calculated mass for $C_{118}H_{206}N_{28}O_{39}$: 2641.1; found: 2641.9.
Figure S26. ESI-MS analysis of **6**.

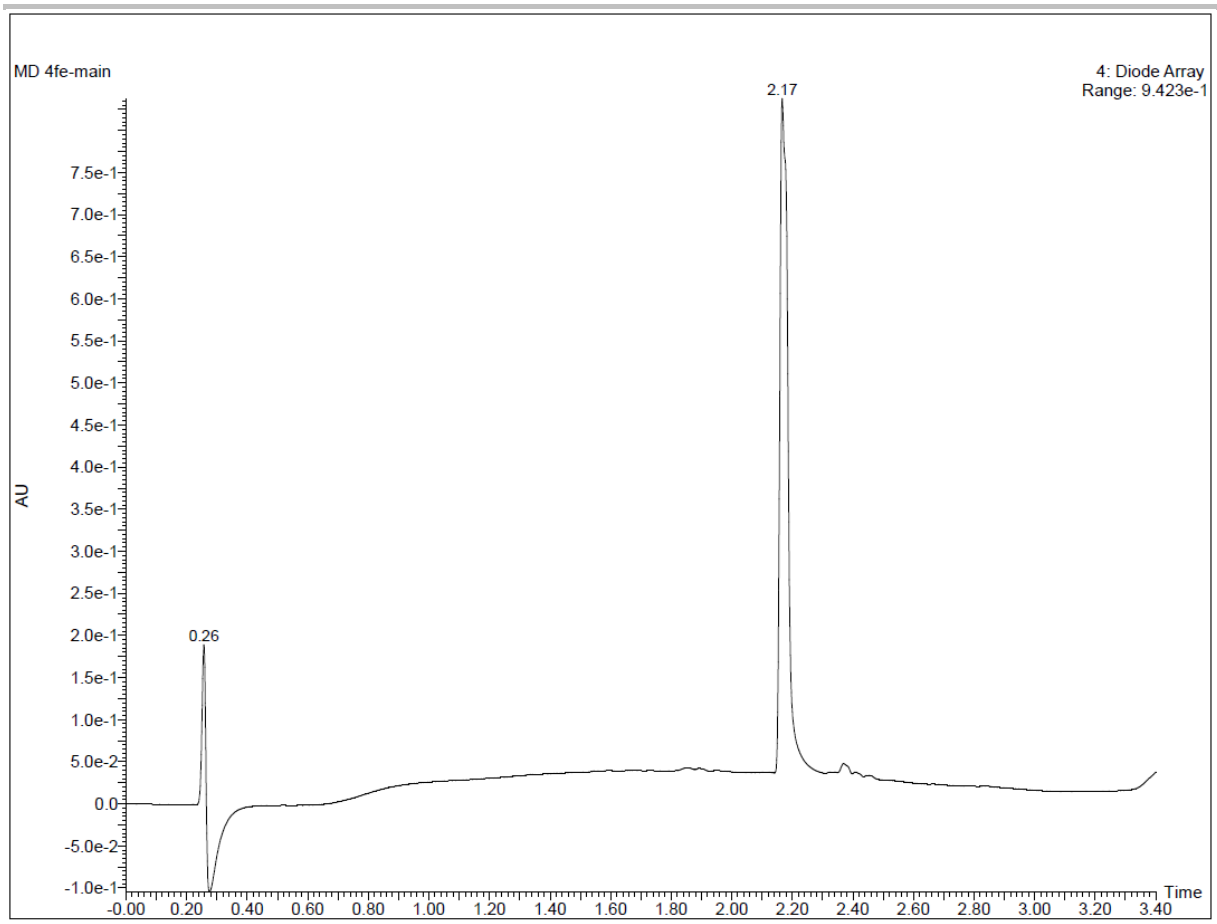

Figure S27. RP-HPLC profile of **5**.

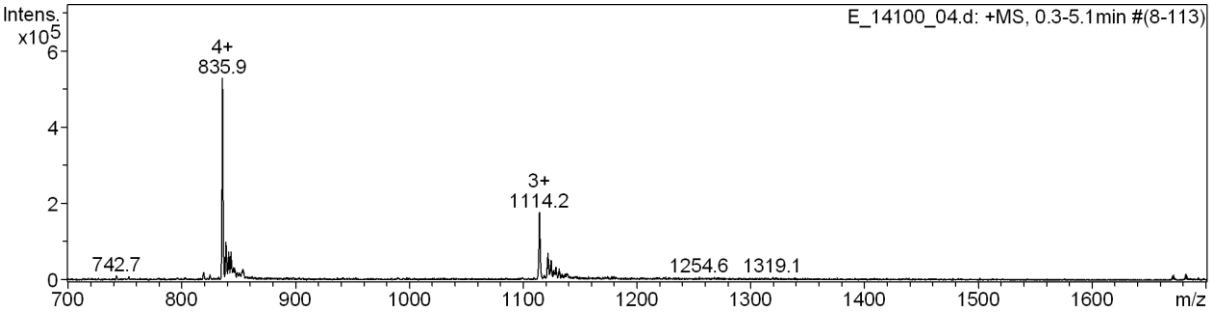

Mass spectrum (ESI, positive mode) calculated mass for $C_{157}H_{242}Fe_4N_{26}O_{39}$: 3341.6; found: 3340.4.
Figure S28. ESI-MS analysis of **5**.

Regeneration of β-CD SAM was performed by using a fresh solution of 0.5 mM oxidized ferrocenyl methanol (Fc-OH). The regeneration is based on the chemical oxidation of complexed β-CD/ferrocene by ferrocenium (oxidized Fc-OH). It is well known that the oxidation of ferrocene to ferrocenium ($Fc^{\cdot+}$) induces the dissociation of the inclusion complex formed with β-CD. (M. J. W. Ludden, D. N. Reinhoudt, J. Huskens, Chem. Soc. Rev. , 2006, 35, 1122–1134). To this end, we prepared a 0.5 mM $Fc^{\cdot+}$-OH solution from the electrolysis of 0.5 mM Fc-OH solution at 0.4Vvs AgCl/Ag). Fig. S29A shows the cyclic voltammograms of Fc-OH solution recorded on glassy carbon electrode before the electrolysis (red curve) and after the electrolysis (blue curve).

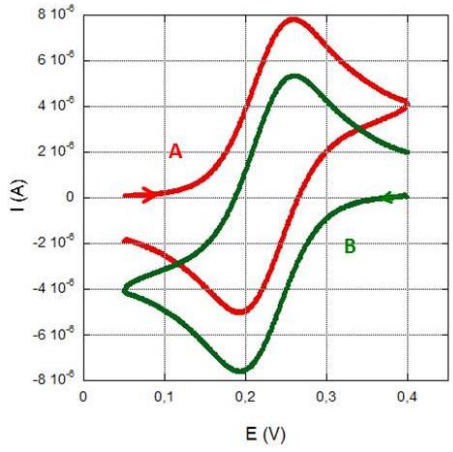

A

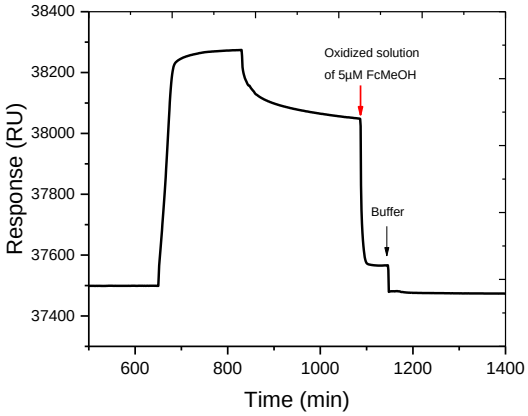

B

Figure S29. (A) cyclic voltammograms of 0.5 mM Fc-OH solution (Tris buffer) recorded on glassy carbon electrode (Φ 3mm) before the electrolysis (red curve, A) and after the electrolysis (blue curve, B). The arrows mark the initial potential scan direction (Scan rate 0.1 V/s). (B) SPR sensorgram of compound **4** adsorption on β-CD SAM and regeneration of step using fresh solution of 0.5 mM oxidized Fc-OH.

References:

[1] M. Mammen, S-K. Choi, G.M. Whitesides, Angew. Chem. Int. Ed. 1998, **37**, 2754-2794.
[2] J. Huskens, A. Mudler, T. Auletta, C. A. Nijhuis, M. J. W. Ludden, D. N. Reinhoudt, J. Amer. Chem. Soc. 2004, **126**, 6784-6797.
[3] A. Grassin, M. Jourdan, P. Dumy, D. Boturyn, *ChemBioChem* **2016**, 17, 515-520.